Thermochemical and Thermophysical Properties of JP-10

Thomas J. Bruno
Marcia L. Huber
Arno Laesecke
Eric W. Lemmon
Richard A. Perkins

Thermochemical and Thermophysical Properties of JP-10

Thomas J. Bruno
Marcia L. Huber
Arno Laesecke
Eric W. Lemmon
Richard A. Perkins

Physical and Chemical Properties Division
Chemical Science and Technology Laboratory
325 Broadway
Boulder, CO 80305

Contents

Thermochemical and Thermophysical Properties of JP-10

MIPR F4FBEY5102G001

Report Prepared for:

Dr. Tim Edwards
Fuels Branch, Turbine Engine Division
Propulsion Directorate, AFRL
Wright Patterson Air Force Base
Ohio, 45433-7103

By:

Physical and Chemical Properties Division
National Institute of Standards and Technology
Boulder, CO 80305

October 2005

Technical Contact:
Dr. Thomas J. Bruno
303-497-5158 (office)
303-497-5927 (fax)
303-497-5978 (laboratory)
bruno@boulder.nist.gov

Administrative Contact:
Ms. Beverly Armstrong
303-497-3868 (office)
303-497-5044 (fax)
beverly@boulder.nist.gov

Executive Summary:

- Report of the chemical analysis of JP-10, on the sample received from AFRL.
- Report of chemical decomposition kinetics of JP-10, on the sample received from AFRL.
- Report of density survey measurements of JP-10, on the sample received from AFRL.
- Report of viscosity survey measurements of JP-10, on the sample received from AFRL.
- Report of speed of sound survey measurements of JP-10, on the sample received from AFRL.
- Report of thermal conductivity survey measurements of JP-10, on the sample received from AFRL.
- Report of the distillation curve of JP-10, on the sample received from AFRL.
- Report on model development for JP-10.

Technical Contact:
Dr. Thomas J. Bruno
303-497-5158 (office)
303-497-5927 (fax)
303-497-5978 (laboratory)
bruno@boulder.nist.gov

Administrative Contact:
Ms. Beverly Armstrong
303-497-3868 (office)
303-497-5044 (fax)
beverly@boulder.nist.gov

Thermochemical and Thermophysical Properties of JP-10

Thomas J. Bruno

Physical and Chemical Properties Division
National Institute of Standards and Technology
Boulder, CO 80305

This report describes measurement and modeling efforts performed on the missile fuel, JP-10. Measurements* include chemical analysis, thermal decomposition kinetics, density, viscosity, speed of sound, thermal conductivity and vapor pressure (distillation curve measurement). These measurements and data from the literature were then used in the formulation of a Helmholtz energy model to describe the equilibrium (thermodynamic) properties, and a corresponding states model for the transport properties.

Keywords**:** density, distillation curve, Helmholtz energy model, JP-10, speed of sound, thermal conductivity, thermal decomposition, vapor pressure, viscosity

Introduction

The Fuels Branch of AFRL (Wright Patterson Air Force Base) required physical property measurement and modeling on an aviation turbine fuel, JP-10. This fluid is essentially a pure component: exo-tetrahydrodicyclopentadiene (tricyclo[$5.2.1.0^{2,6}$]decane, CAS No. 2825-82-3). This fluid has an appreciable density (0.94 g/cm^3), and produces a specific impulse of 297.4 s (the thrust per mass flow rate at the nozzle). These characteristics, as well as the very low freezing point of the fluid (−79 °C) has made this fluid the only air- breathing missile fuel used by the United States at the present time. The chemical structure of this fluid is shown in Figure 1. To achieve the goal of producing a provisional or preliminary physical property model, measurements of chemical composition, thermal decomposition, density, viscosity, thermal conductivity, speed of sound, and vapor pressure were carried out. These data were then used, along with evaluated data from the literature, to develop the model. The major accomplishments of this project are summarized in this report.

Note:
In order to describe materials and experimental procedures adequately, it is occasionally necessary to identify commercial products by manufacturers' names or labels. In no instance does such identification imply endorsement by the National Institute of Standards and Technology, nor does it imply that the particular product or equipment is necessarily the best available for the purpose.

Chemical Analysis of JP-10

Two containers of JP-10 were obtained from AFOSR, Fuels Branch, for testing. There were no identifying marks or numbers listed on the containers beyond the chemical name and contact information of Tim Edwards, Fuels Branch, AFOSR.

A 1 mL aliquot was withdrawn from one of the containers for analysis. Sample was not permitted to come into contact with the can exterior. The sample was maintained in a sealed scintillation vial throughout the course of this work. Exposure of the sample to ambient air was minimized to prevent oxidation and the uptake of moisture. Although the vial was stored at 7 °C when not in use, the sample was permitted to attain room temperature before the vial was opened for use.

A gas chromatography-mass spectrometry method was used for the analysis. A 30 m capillary column with a 0.1 μm coating of 5 % phenyl polydimethyl siloxane was chosen as the stationary phase. This phase provides separations based upon boiling temperature and also on polarity. It is considered a weakly polar stationary phase. Sample was injected manually via chromatographic syringe into a split/splitless injector that was set with a 100 to 1 split ratio. The injector was operated at a temperature of 350 °C and held to a constant head pressure of 68.77 kPa (10 psig). The column was temperature programmed to provide complete and rapid elution with minimal loss of peak shape. Initially, the temperature was maintained isothermally at 60 °C for 2 min, followed by a 2 °C/min ramp to 90 °C, followed by a 10 °C/min ramp to 250 °C. Although the analysis was allowed to run for 40 min, all peaks of interest were eluted after approximately 7 min. These conditions proved to be suitable for most of the constituents, which produced sharp, clearly defined peaks.
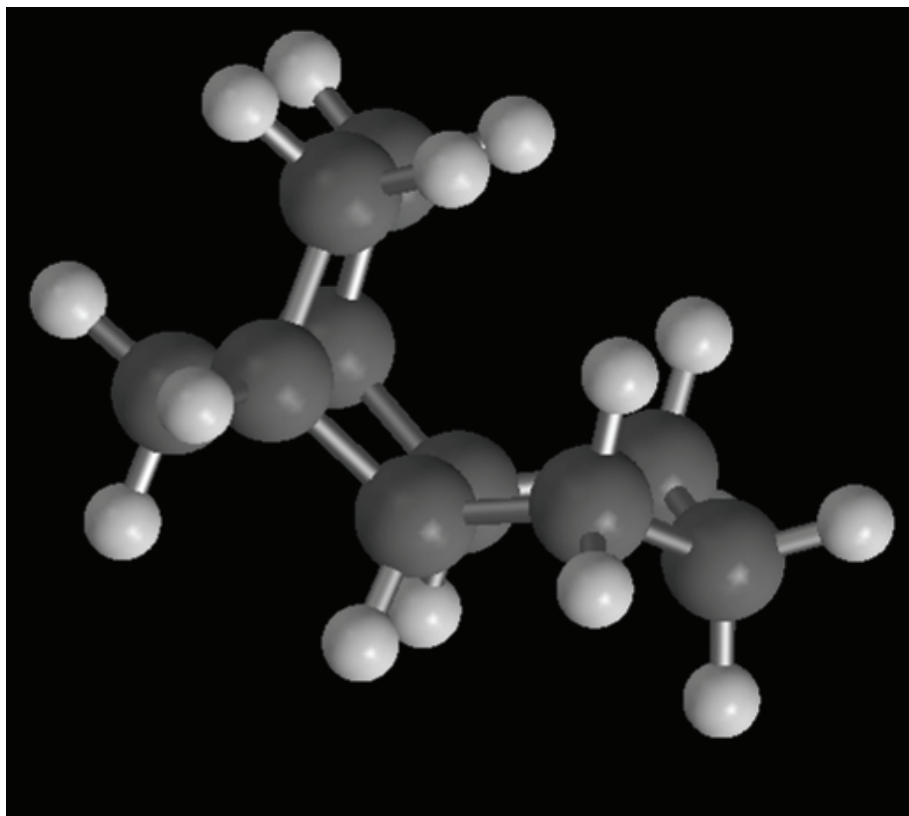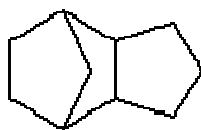
Figure 1. The chemical structure of JP-10, exo-tetrahydrodicyclopentadiene (tricyclo[5.2.1.0^{2,6}]decane), depicted in a traditional planar format and a three-dimensional ball and stick format.

The total ion chromatogram for this analysis is presented in Figure 2. The major constituent of the sample is exo-tetrahydrobicyclopentadiene, or JP-10. In addition, two major related impurities were identified. Both elute after the main peak of JP-10. The first impurity is identified as adamantane, and the second is identified as the endo- isomeric modification of JP-10 (hereafter referred to as endo-). The approximate (uncalibrated) composition is:

Table 1. Major components identified in sample of JP-10 provided by Wright Laboratory.

Constituent	Percent, mass/mass
JP-10	96.5
adamantane	1.0
endo-	2.5

There is a peak whose mass spectrum is consistent with decahydronaphthalene that elutes immediately before the main JP-10 peak. It was not quantitated separately because it was not base-line resolved from the main JP-10 peak. It is possible to magnify the very light components that elute before the major constituents. The magnified section of the total ion chromatogram is presented in Figure 3. Numerous additional peaks can be seen, not all of which can be identified. The following table provides the likely identities of some of the larger minor constituents:

Table 2. Early eluting components in the analysis of JP-10.

Peak	Name
A	2-methyl-bicyclo[3.2.1]octane
B	2-ethyl-bicyclo[2.2.1]heptane
C	endo-2,2,3-trimethyl-bicyclo[2.2.1]heptane
D	cis-1-methyl-4-(-1-methylethenyl)cyclohexane
E	2,6-dimethyl-bicyclo[3.2.1]octane

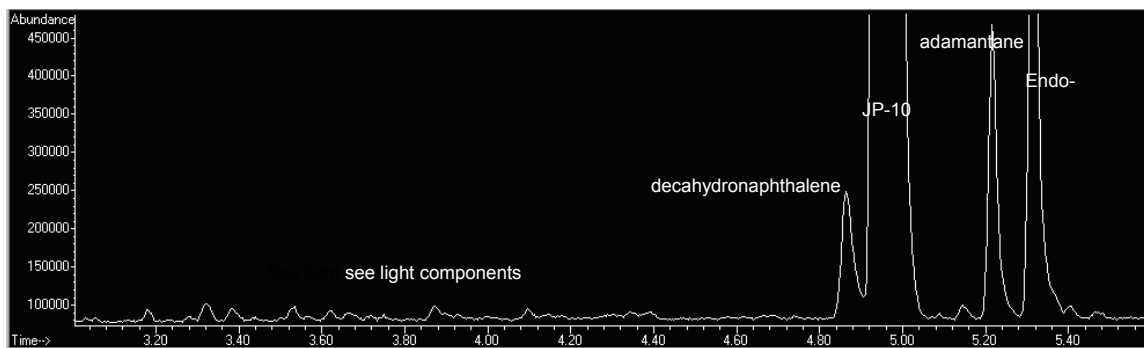The peak labels correspond to the identified peaks of Figure 3.

Figure 2. Total ion chromatogram of a sample of pure JP-10, as received from Wright Laboratory.
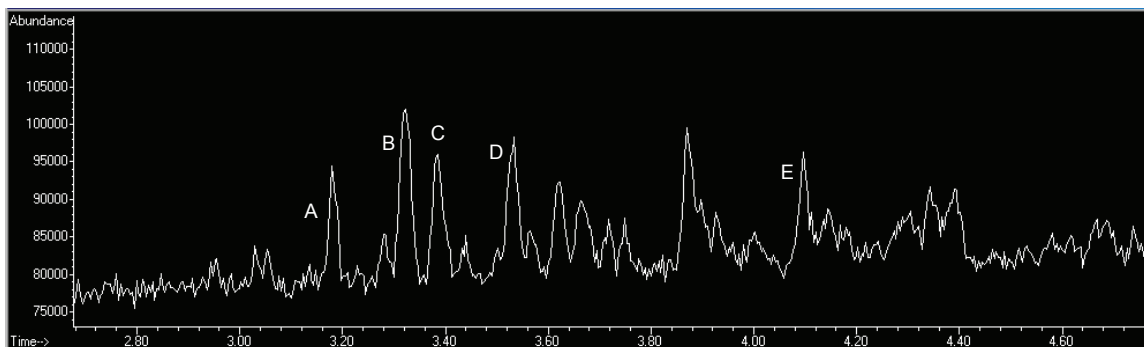

Figure 3. Total ion chromatogram, magnified, for the light components (early eluting peaks).

Thermal Decomposition of JP-10

Several studies have been done to address the thermal decomposition of JP-10[1-8]. These studies have been done in various test rigs that have been designed to mimic conditions that are applicable in engines. Typically, residence times are very short, in the range of milliseconds to several min. The longer residence times (between 1 and 48 hours) normally associated with the measurement of thermophysical properties required us to address the topic of thermal decomposition from a more fundamental standpoint. We must approach the question of thermal decomposition in such a way as to provide a predictive capability for property measurement time scales[9,10].

For a simple reaction in which a starting material (A) thermally decomposes into a product (eq. 1), perhaps the best description of the decomposition is the fundamental rate equation. For a model reaction where starting material A decomposes into product B (eq. 1), the rate law can be written as eq. (2) or (3):

$$A \rightarrow B \tag{1}$$
$$\text{Rate} = -d[A]/dt \tag{2}$$
$$\text{Rate} = d[B]/dt, \tag{3}$$

where [A] is the concentration of A, [B] is the concentration of B, and t is the time. As the reaction proceeds, the decrease in A (denoted by the negative sign) is accompanied by a corresponding increase in B, and a rate equation can be expressed in terms of the reaction products as:

$$d/dt\ [B] = k[B]^n, \tag{4}$$

where k is the reaction rate constant and n is the order of the reaction. If we integrate the equation and assume first order, we obtain:

$$\ln[B] - \ln[B_o] = kt, \tag{5}$$

where $[B_o]$ is the initial product concentration, which at the start of a decomposition reaction, is zero. A plot of ln[B] as a function of time will provide a straight line with a zero intercept, the slope of which is k.

An inherent limitation in defining the rate constant in terms of B occurs for disproportionate reactions, where each molecule of starting material decomposes to generate more than one molecule of product. A disproportionate reaction can be written as: $A \rightarrow \Sigma B_i$, where B_i is the number of individual products formed in the reaction. In the thermal decomposition of a complex fluid, the potential for such a situation is clear. Furthermore, the decomposition rate of a single component can be significantly altered in the presence of the mixture compared to the pure component [3]. Nevertheless, insight can be gained into the overall fluid stability against thermal stress by focusing instead on the global behavior of the bulk fluid. Then, if the trends in the measured data are appropriate, the decomposition can be approximated as first-order decomposition [11]. Thus, rather than describing the decomposition of each component in the mixture, a global rate constant can be used to describe the bulk behavior of the complex fluid

[12,13]. This is the approach we have taken in the assessment of the thermal decomposition of JP-10.

The simple apparatus assembled to make the thermal decomposition kinetics measurements consists of a 304L (AISI designation) stainless-steel thermal block that is heated to the desired experimental temperature. In the work reported here, temperatures between 350 and 425 °C were used. Stainless-steel was chosen for the block because of its favorable mechanical and corrosion resistance properties at high temperature. The block is supported in an insulated box with carbon rods, which were chosen for low thermal conductivity. The temperature is maintained and controlled (by a PID controller) to within 0.1 °C in response to a platinum resistance sensor embedded in the thermal block and sealed with ceramic adhesive. The cells consist of 6.4 cm lengths of ultrahigh pressure 316L stainless steel tubing (0.64 cm external diameter, 0.18 cm internal diameter) that are sealed on one end with a stainless-steel plug welded by a clean tungsten-inert-gas (TIG) process. Each cell is connected to a high-pressure valve at the other end with a short length of 0.16 cm diameter 316 stainless steel tubing with an internal diameter of 0.02 cm. This length of tubing is also TIG welded to the cell. Each cell and valve is capable of withstanding a pressure in excess of 105 MPa at the desired temperature. Although not used in the experiments described here, an impact agitator is attached to the heating block for use when heterogeneous systems are investigated.

The internal volume of each cell (including the short length of connecting tubing, and the small dead volume of the valve) was determined by gravimetric gasometry using liquid carbon dioxide. This procedure consisted of filling a cell of known mass with carbon dioxide to a predetermined pressure (20.68 MPa) and at a constant temperature. The cell mass was measured again and the increase in mass allowed calculation of the cell volume using an accurate equation of state for the density of carbon dioxide [14]. Cell volumes were measured three times and averaged to yield 0.210 ± 0.002, 0.226 ± 0.001, and 0.235 ± 0.003 cm^3 for the three vessels.

The cell filling procedure was a critical step since we desired to mimic the conditions that might be encountered in our physical property measurement apparatus. We modified a computer program that provides the necessary fluid mass to achieve a selected pressure at the desired temperature [14]. This program allowed us to determine the target mass to place in the evacuated cell, given the cell volume, to achieve a nominal 34.5 MPa at temperatures between 350 and 425 °C. A simple predictive equation of state for exo-tetrahydrobicyclopentadiene (JP-10) was used to estimate the pressure in each cell at the decomposition temperature [14].

The calculated mass of JP-10 was added to the cell with a syringe equipped with an ultra fine needle, and the mass of the cell was measured to within ±0.0001 g. The valve was then affixed to the cell and sealed. Sample masses were typically on the order of 0.1 g and varied depending on the experimental temperature and cell volume. Cells were then chilled to −196 °C in liquid nitrogen and subsequently evacuated to 10 Pa through the valve to remove air from the cell. The valve was then closed and the cell was warmed to room temperature, at which time the mass of the entire cell-valve assembly was recorded.

Loaded cells were then inserted into the stainless steel thermal block that was heated to the desired experimental temperature. The cells were maintained at the reaction temperature for a specified period of time ranging from 4 min to 20 h. After the desired time period, the cells were

removed from the thermal block and quenched in water at room temperature. The cells were dried and the mass was measured to ensure that no leakage had occurred over the course of the experiment. The thermally stressed JP-10 was then recovered from the cells and analyzed.

After each run, the cells and valves were solvent-rinsed with hexanes, toluene, acetone, and finally methanol using an ultra fine needle. Solvent rinsing was performed until each solvent was colorless as it exited the cell. Cleaned cells and valves were heated to 150 °C for at least 30 min to remove residual solvent.

A blank experiment was performed to investigate any possible artifacts introduced in the experiment such as residual solvent in the cell or possible catalytic behavior of the cell materials. The cells were loaded and evacuated as described above, then maintained at room temperature for 65 h. The liquid sample was then removed and analyzed in the same manner as the samples that had been exposed to elevated temperature.

The purpose of the analytical procedure mentioned above was to measure the decomposition kinetics of the thermally stressed JP-10. As such, a detailed identification of each product is unnecessary; only the rate of change is required. A liquid sampling procedure was developed to minimize sample loss when the cells were opened. A short length of stainless steel tubing was connected to the valve outlet and placed inside a pre-chilled (at 7 °C) glass vial. The valve was slowly opened and the reacted JP-10 was expelled and collected in the vial. The cell was then removed from the valve, and any sample remaining in the cell was transferred to the glass vial using a syringe equipped with an ultra-fine needle. Samples were refrigerated (at 7 °C) until the analysis was performed. Liquid samples were prepared for gas chromatographic analysis by dilution in n-dodecane. The resulting solution was typically 8 % reacted JP-10, mass/mass. The uncertainty in the mass measurement was 0.0001 g. Sample vials were crimp sealed and the contents were mixed using a vortex mixer.

Aliquots (2 µL) of the sample were injected into a gas chromatograph equipped with an automatic sampler and a flame ionization detector. Research-grade nitrogen was used as the carrier and make-up gas. The split/splitless injection inlet was maintained at 300 °C and samples were separated on a capillary column (30 m column coated with a 1 µm film of 100 % dimethylpolysiloxane). A temperature program was used consisting of an initial isothermal separation at 100 °C for 2 min followed by a 7 °C/min gradient to 225 °C. This final temperature was held constant for 15 min.

Chromatographic analysis was performed on a suite of emergent decomposition peaks. These were peaks corresponding to products formed during the thermal stress; they were not present in the unreacted JP-10. Retention times from a standard solution of n-alkanes were used to account for the day-to-day variations in the retention times of the decomposition products. This was done with a mixture of n-hexane, n-heptane, n-octane and n-nonane that was analyzed before and after each JP-10 sample. Retention times of the reference alkanes were used to bracket and predict the retention times of the major decomposition products, and were remarkably consistent throughout this study. A linear regression was used to fit the data and typically yielded correlation coefficients greater than 0.99999, and predicted retention times were typically within ±0.01 min of the measured product retention times. This procedure ensured that no extraneous peaks were used in the chemical analyses upon which the reaction kinetics were based.

An external standard of n-hexane in a solution of n-tetradecane was used to account for variation in sample response from day to day. This external standard was injected before and after each set of analytical samples of thermally stressed JP-10. The chromatographic areas adjusted with this calibration are represented as Ac. A plot of ln(Ac) against time for each temperature was used to determine the rate constants for the decomposition.

The thermal decomposition peaks that were obtained with the ampoule procedure described above were, in general, faster-eluting than the main JP-10 peaks. Some later eluting peaks were found. Among the later eluting peaks that were not part of the starting material were: 1,1'-bicyclopentyl, 1-cyclopentylcyclopentene, and 2,3-dihydro-5-methyl-1H-indene. These are not considered further since they were not used in determining the thermal decomposition rate.

The major early eluting peaks are shown in the total ion chromatogram that is presented as Figure 4. These measurements were made after the sample was maintained at 425 °C and 34 MPa for 90 min. The labels on this figure correspond to the components identified in Table 3.

Table 3. A listing of the components labeled on the total ion chromatogram presented in Figure 4. These components have been identified on the basis of their mass spectra, after a sample of JP-10 was maintained at 425 °C and 34 MPa for 90 min.

Component	Name
1	n-propane
2	n-butane
3	cyclopentane
4	methyl cyclopentane
5	1-methyl cyclopentene
6	benzene
7	ethyl cyclopentane
8	ethylide cyclopentane
9	toluene
10	n-propyl cyclopentane
11	cis-bicyclo[3.3.0]oct-2-ene
12	ethyl benzene
13	o-xylene
14	octahydropentylene
15	3-methyl cyclo octane

As an example of the decomposition data, the plot of lnAc against time for 375 °C is provided in Figure 5.

The preliminary results for the decomposition reaction rate constants are provided in Table 4. These rate constants may change as the data analysis is finalized. In this table, k is the pseudo first-order rate constant given in min^{-1}. The uncertainty, obtained from linear regression of ln Ac against time, and the coefficient of variation in percent is also provided.

Table 4. Thermal decomposition reaction rate constants for JP-10.

Temp, °C	Temp, K	k, min^{-1}	std. error	CV, %
425	698	0.01518	0.00302	19.9
400	673	0.00437	0.00039	9.02
375	648	0.00111	0.00016	14.4
350	623	0.00024	0.00004	17.46

The curvature that can be seen in the measurements of Figure 5 is indicative of disproportination, or the subsequent reaction of reaction products. This invalidates a strictly first order approach to the analysis of the rate, but it does not affect the interpretation in the context of this study. Recall that our purpose here is to delineate the regions in which thermophysical properties can be measured in laboratory apparatus.
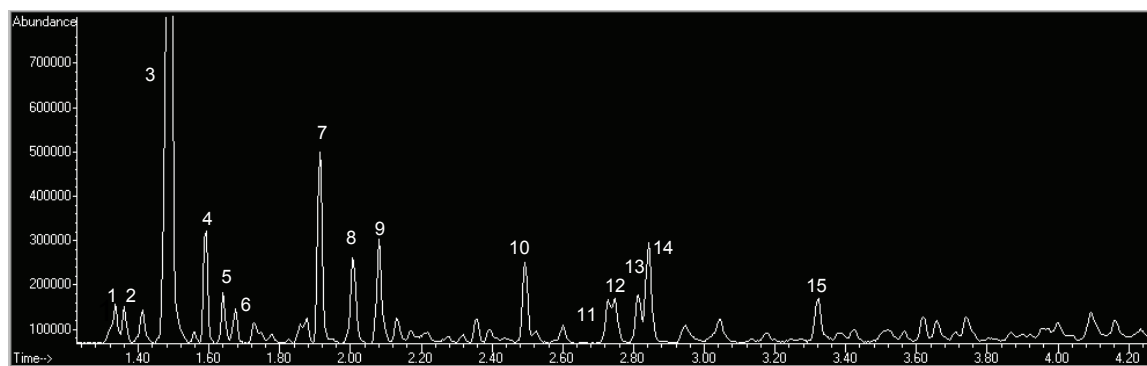
Figure 4. A total ion chromatogram showing the early eluting peaks of decomposed JP-10, harvested after 90 min at 425 °C and 34 MPa.
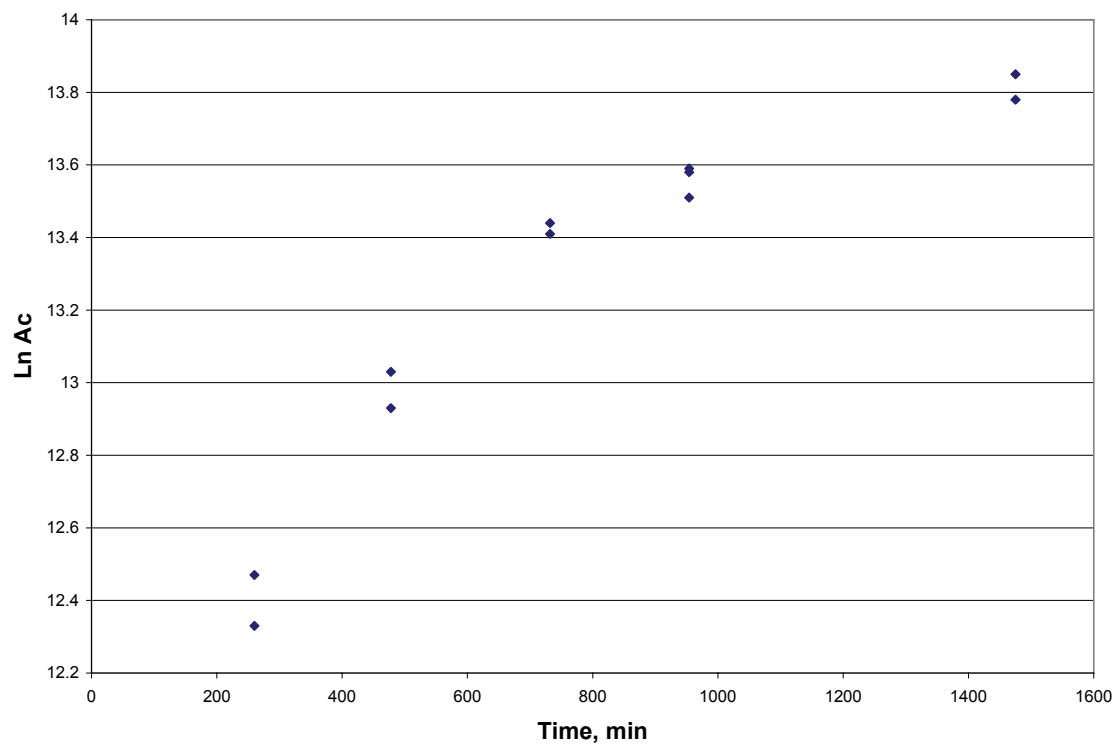
Figure 5. Representative measurements of the decomposition of JP-10, measured at varying times at a temperature of 375 °C. Ln(Ac) is the natural logarithm of the calibrated chromatographic area measured for each ampoule sample.
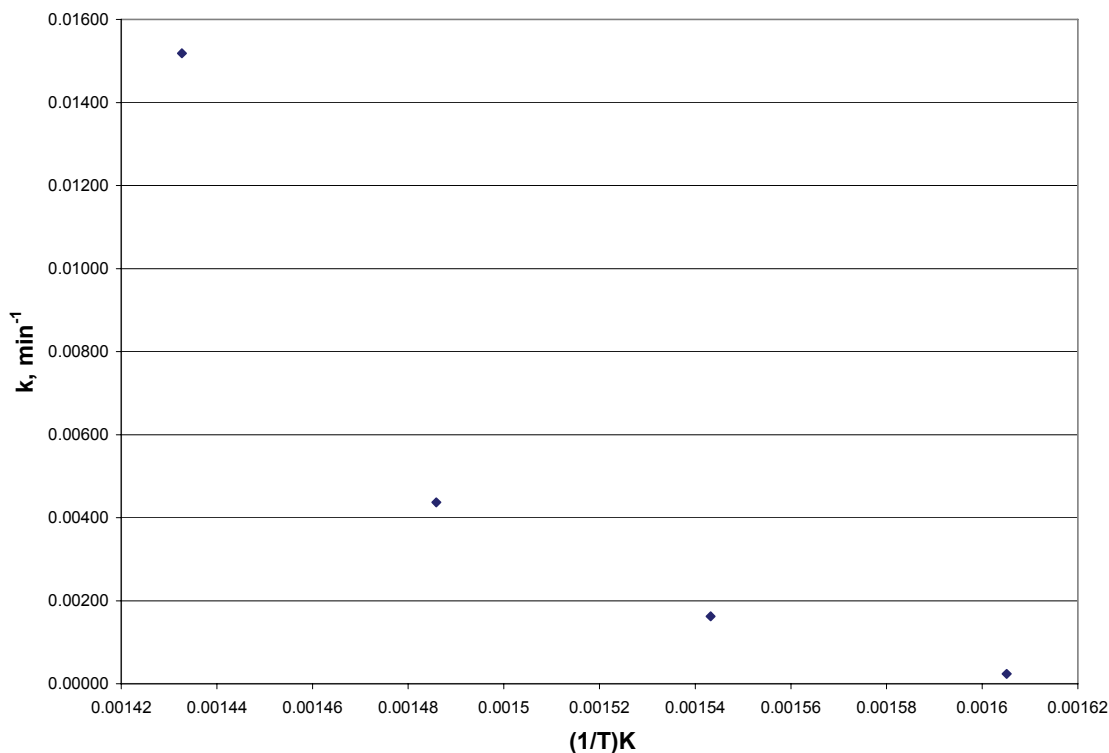
Figure 6 Temperature dependence of the measured thermal decomposition rate constants.

The temperature dependence of the measured rate constants is provided in Figure 6. Here again the curvature is indicative of disproportionation.

It is difficult or impossible to directly compare the thermal decomposition results presented here with previous results since most previous studies used very short residence times. Previous studies employed residence times as short as milliseconds to as long as 4 s. In this work, the residence times were much longer, since the context of these measurements was indeed different. Here, at the highest temperature studied (425 °C), the shortest residence time was 2220 s. At the lowest temperature studied, 350 °C, the longest residence time used was 241,000 s.

For the purpose of thermophysical property measurement, residence time in instrumentation is not expected to be a factor unless the fluid is exposed to temperatures between 375 and 400 °C. All of the measurements in this work were made at temperatures considerably below this temperature. Thus, we may conclude that thermal decomposition is not an issue with these measurements.

The onset of thermal decomposition does not necessarily preclude measurements at higher temperatures. It simply means that above 375 °C, explicit consideration must be given to the potential of sample decomposition. Test samples must be analyzed after each measurement, and residence times must be limited.

Instrumentation for Density, Viscosity, and Speed of Sound Measurements

The density, viscosity, and speed of sound of a JP-10 sample from Wright Laboratory were measured in two commercial rapid characterization instruments. A Stabinger viscodensimeter (Anton Paar SVM 3000) was used to determine the density and the absolute and kinematic viscosity in the temperature range from −40 °C to 100 °C (233.15 K to 373.15 K) at atmospheric pressure. A sound-speed analyzer (Anton Paar DSA 5000) was used to measure the speed of sound and the density of the JP-10 samples at atmospheric pressure (84 kPa at 1654.7 m altitude of Boulder, Colorado) in the temperature range from 5 °C to 70 °C (278.15 K to 343.15 K).

The measurements with the Stabinger viscodensimeter were carried out according to ASTM Standard D 7042 – 04 *Standard Test Method for Dynamic Viscosity and Density of Liquids by Stabinger Viscometer (and the Calculation of Kinematic Viscosity)*. The following instrument description is partly excerpted from ASTM Standard D 7042 – 04. The viscometer part of the instrument uses a rotational coaxial cylinder measuring system. The outer cylinder (tube) of Hastelloy is driven by a motor at a constant and known rotational speed. The low-density inner cylinder (rotor) of titanium is held in the axis of rotation by the centrifugal forces of the higher density sample and in its longitudinal position by the magnet and the soft iron ring. Consequently, the system works free of bearing friction as found in rotational viscometers. A permanent magnet in the inner cylinder induces eddy currents in the surrounding copper casing. The rotational speed of the inner cylinder establishes itself as the result of the equilibrium between the driving torque of the viscous forces and the retarding eddy current torque. This rotational speed is measured by an electronic system (Hall effect sensor) that counts the frequency of the rotating magnetic field (see Figures 7 and 8).

The digital density analyzer in the viscodensimeter uses a U-shaped vibrating sample tube and a system for electronic excitation and frequency counting. The density of the sample liquid in the vibrating tube is obtained from the resonant frequency of the vibrating system relative to the resonant frequency with a calibration liquid of known density.

The combination of a viscometer and a densimeter makes it possible to obtain absolute viscosity η as well as kinematic viscosity ν of a sample because $\nu = \eta/\rho$, where ρ is the density. The amount of sample needed for both measuring cells is less than 5 mL.

The assembly is thermostatted by a copper block that surrounds both the viscosity and the density measuring cells and keeps both cells at the same temperature. A thermoelectric heating and cooling system ensures the temperature stability of the copper block within 0.005 °C from the set temperature at the position of the viscosity cell over the whole temperature range. At temperatures below 0 °C the viscodensimeter was cooled with an additional external circulator. The uncertainty ($k = 2$; 95 % confidence level) of the temperature calibration is no more than 0.03 °C over the range from 15 to 100 °C. Outside this range the calibration uncertainty is no more than 0.05 °C.
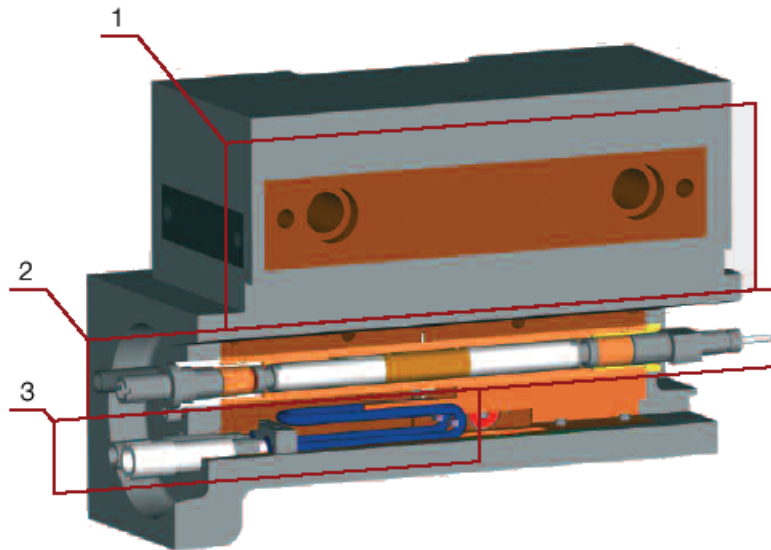
Figure 7. Main components of the Stabinger viscodensimeter SVM 3000.
1 – Thermostatting Peltier block, 2 – Concentric cylinder viscometer, 3 – Vibrating tube densimeter.
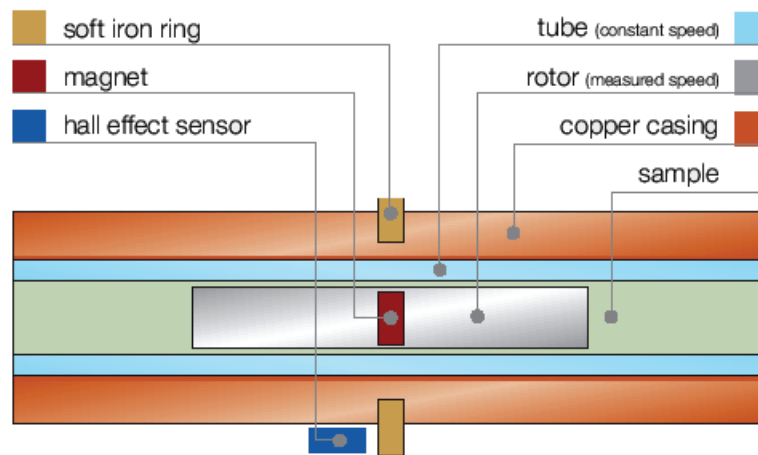
Figure 8. Assembly of the concentric cylinder viscometer in the Stabinger viscodensimeter SVM 3000.

The uncertainty of the viscosity measurement is stated by the manufacturer as 0.35 % of the measured value and that of the density measurement at 0.5 kg·m^{-3}, while the repeatabilities are 0.2 % of the measured value and 0.2 kg·m^{-3}, respectively. However, wide-ranging comparisons of measured viscosities with reference values of viscometer calibrating liquids both in this laboratory and elsewhere have shown that the uncertainty of the viscosity measurements as stated by the manufacturer is not maintained throughout the entire advertised measuring range of the instrument (0.2 to 10,000 mPa·s in absolute viscosity and 0.2 to 10,000 mm^2·s^{-1} in kinematic viscosity) with one calibration. The actual uncertainty in these measurements has been assessed

15

by benchmark measurements on two standard oils. These tests will be discussed in the section on JP-10 viscosity measurements.

Density and the speed of sound in liquid samples of JP-10 were measured with a sound-speed analyzer DSA 5000 that is similar to the SVM 3000 viscodensimeter in design and appearance. It includes also a vibrating U-tube densimeter and a pulse-echo speed of sound measurement cell that is illustrated below. However, the temperature range is limited from 0 °C to 70 °C. The measurement uncertainty is stated for both properties as 0.01 % to 0.1 %, with repeatabilities of 0.001 kg·m^{-3} in the density and 0.1 m·s^{-1} in the speed of sound measurement. The density measurement in the DSA 5000 is more accurate than that in the viscodensimeter. By design, the densimeter in the viscodensimeter was made only as accurate as necessary in view of the higher uncertainty of the viscosity measurement.

Combining a densimeter with a speed of sound measurement (Figure 9) makes it possible to obtain the adiabatic compressibility $\kappa_s = -(\partial V/\partial p)_s/V = 1 / (\rho\, w^2)$ where V denotes volume, p is pressure, and w the speed of sound. Subscript s indicates "at constant entropy s."
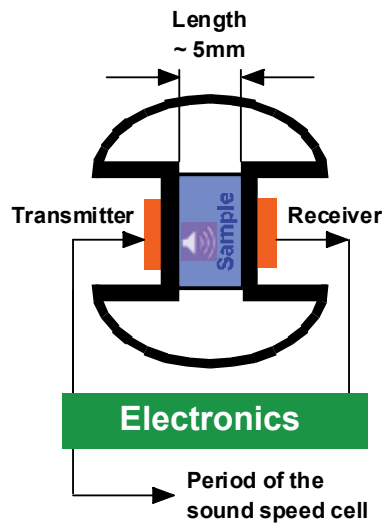
Figure 9. Schematic of the sound speed measurement in the DSA 5000.

Density Measurements for JP-10

The density of JP-10 was measured in both instruments, the Stabinger viscodensimeter SVM 3000 as well as the Sound Speed Analyzer DSA 5000. The results are tabulated in Table 5 and in Table 6, and illustrated in Figure 10.
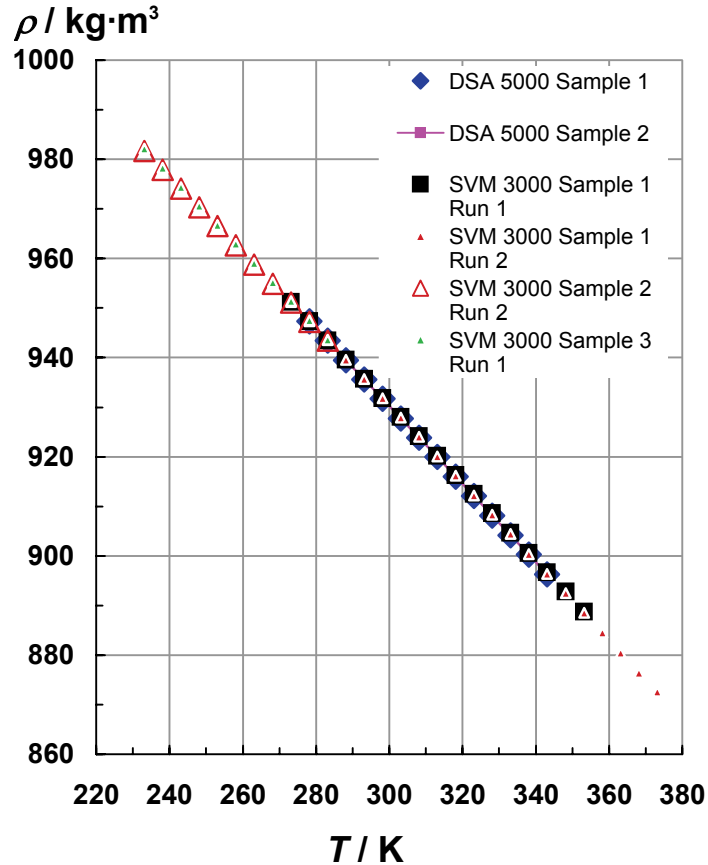
Figure 10. Densities of JP-10 measured in the Stabinger viscodensimeter and in the sound speed analyzer DSA 5000.

The experimental data were correlated by a quadratic polynomial in reduced temperature

$$\rho = a_0 + a_1 T_{\mathbf{r}} + a_2 T_{\mathbf{r}}^2, \tag{6}$$

where ρ is the density in kg·m^{-3} and $T_r = T / (273.15 \text{ K})$ is the reduced absolute temperature. The values of the parameters a_0 to a_2 were determined by linear least squares regression. They are listed with their standard deviations in Table 7. The experimental density data are represented by eq. (6) with a maximum negative deviation of -0.02 % and a maximum positive deviation of 0.04 %. These deviations are within the estimated uncertainty of the data. The percent deviations are illustrated in Figure 11, which gives also an indication of the repeatability of either

instrument and of their mutual agreement. The data show the higher repeatability and lower uncertainty of the vibrating tube densimeter in the sound speed analyzer DSA 5000.

Table 5. Densities of JP-10 measured in the Stabinger viscodensimeter SVM 3000. The ambient pressure during the measurements was 84 kPa.

Temp-erature T	Density ρ	Temp-erature T	Density ρ	Temp-erature T	Density ρ	Temp-erature T	Density ρ
K	kg·m^{-3}	K	kg·m^{-3}	K	kg·m^{-3}	K	kg·m^{-3}
Sample 1 Run 1		*Sample 2 Run 1*		*Sample 2 Run 2*		*Sample 3 Run 1*	
353.15	888.7	373.15	872.6	283.15	943.4	283.15	943.6
348.15	892.8	368.15	876.4	278.15	947.2	278.15	947.5
343.15	896.7	363.15	880.5	273.15	951.1	273.15	951.4
338.15	900.6	358.15	884.5	268.15	954.9	268.15	955.2
333.15	904.6	353.15	888.5	263.15	958.8	263.15	959.1
328.15	908.6	348.15	892.5	258.15	962.6	258.15	962.9
323.15	912.5	343.15	896.4	253.15	966.5	253.15	966.7
318.15	916.3	338.15	900.4	248.15	970.3	248.15	970.6
313.15	920.2	333.15	904.4	243.15	974.1	243.15	974.4
308.15	924.1	328.15	908.3	238.15	977.9	238.15	978.3
303.15	928.0	323.15	912.2	233.15	981.7	233.15	982.1
298.15	931.8	318.15	916.2				
293.15	935.7	313.15	920.1				
288.15	939.6	308.15	924.0				
283.15	943.4	303.15	927.9				
278.15	947.3	298.15	931.8				
273.15	951.2	293.15	935.7				
		288.15	939.6				
		283.15	943.5				
		278.15	947.3				
		273.15	951.2				

Table 6. Densities of JP-10 measured in the Sound Speed Analyzer DSA 5000.The ambient pressure during the measurements was 84 kPa.

Temperature T	Density ρ	Temperature T	Density ρ
K	kg·m^{-3}	K	kg·m^{-3}
Run 1		*Run 2*	
343.152	896.276	343.150	896.272
338.151	900.235	338.150	900.232
333.150	904.188	333.150	904.186
328.151	908.134	328.151	908.129
323.149	912.072	323.151	912.068
318.150	916.002	318.150	915.999
313.151	919.923	313.152	919.918
308.151	923.837	308.151	923.833
303.152	927.750	303.151	927.744
298.152	931.664	298.151	931.659
293.151	935.577	293.152	935.573
288.151	939.491	288.151	939.486
283.151	943.403	283.150	943.400
278.147	947.315	278.143	947.311

Table 7. Parameter values and associated standard deviations of the density correlation eq. (6).

i	Parameter a_i	Standard deviation s_i
0	1153.0412	1.020
1	−192.47447	1.868
2	−9.3825928	0.8485

100 ((ρ_{exp}/ρ_{corr}) - 1)
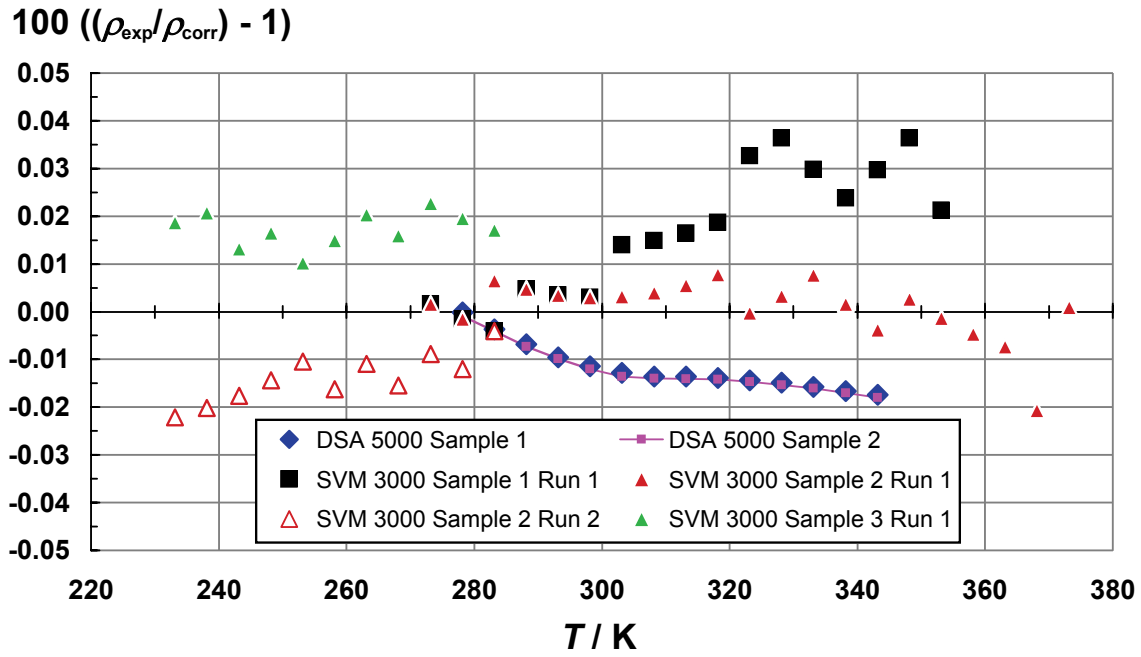
Figure 11. Percent deviations of the measured densities of JP-10 relative to the correlation, eq. (6).

Viscosity Measurements for JP-10

The viscosity of JP-10 was measured with the Stabinger viscodensimeter SVM 3000 on three samples from the same stock to assess the repeatability of the instrument. Four runs were carried out in the combined temperature range from 233.15 K to 373.15 K. The measured absolute and kinematic viscosities are tabulated in Table 8 and illustrated in Figure 12.

The viscosity of two certified viscosity standard calibrating liquids was measured to verify the performance of the viscometer. Calibrating liquids S3 and N1.0 were obtained from Cannon Instruments, Inc. This company has been delegated by NIST to provide U.S. national measurement standards and to issue calibration and measurement certificates for certified liquid viscosity reference standards. Figure 12 shows that the viscosity of standard calibrating liquid N1.0 is about three times lower than that of JP-10 while the temperature dependence is about the same for both liquids in the range where the viscosity of the standard calibrating liquid N1.0 is known. The viscosity of standard calibrating liquid S3 matches that of JP-10 at 373.15 K but increases faster with decreasing temperature and is four times higher at 233.15 K. Thus the viscosities of the two standard calibrating liquids bracket that of JP-10 and allow a rigorous uncertainty assessment of the instrument during these measurements.

Table 8. Absolute and kinematic viscosities of JP-10 measured in the Stabinger viscodensimeter SVM 3000. The ambient pressure during the measurements was 84 kPa.

Temp-erature T	Absolute viscosity η	Kinematic viscosity v	Temp-erature T	Absolute viscosity η	Kinematic viscosity v
K	mPa·s	mm^2·s^{-1}	K	mPa·s	mm^2·s^{-1}
Sample 1 Run 1			**Sample 2 Run 1**		
353.15	1.1619	1.3074	373.15	0.91482	1.0483
348.15	1.2411	1.3901	368.15	0.97140	1.1084
343.15	1.3284	1.4815	363.15	1.0325	1.1726
338.15	1.4252	1.5825	358.15	1.0989	1.2424
333.15	1.5321	1.6937	353.15	1.1713	1.3184
328.15	1.6515	1.8177	348.15	1.2507	1.4014
323.15	1.7848	1.9560	343.15	1.3381	1.4927
318.15	1.9343	2.1109	338.15	1.4347	1.5934
313.15	2.1034	2.2858	333.15	1.5419	1.7049
308.15	2.2957	2.4843	328.15	1.6612	1.8289
303.15	2.5153	2.7105	323.15	1.7948	1.9674
298.15	2.7673	2.9697	318.15	1.9449	2.1229
293.15	3.0582	3.2684	313.15	2.1147	2.2984
288.15	3.3963	3.6148	308.15	2.3080	2.4978
283.15	3.7915	4.0188	303.15	2.5287	2.7251
278.15	4.2564	4.4932	298.15	2.7823	2.9859
273.15	4.8078	5.0547	293.15	3.0752	3.2865
			288.15	3.4161	3.6358
			283.15	3.8149	4.0435

Temp-erature T	Absolute viscosity η	Kinematic viscosity ν	Temp-erature T	Absolute viscosity η	Kinematic viscosity ν
			278.15	4.2857	4.5240
			273.15	4.8444	5.0930
K	**mPa·s**	**mm²·s⁻¹**	**K**	**mPa·s**	**mm²·s⁻¹**
Sample 2 Run 2			**Sample 3 Run 1**		
283.15	3.8094	4.0382	283.15	3.8165	4.0446
278.15	4.2790	4.5174	278.15	4.2932	4.5312
273.15	4.8364	5.0851	273.15	4.8572	5.1056
268.15	5.5038	5.7634	268.15	5.5321	5.7915
263.15	6.3083	6.5794	263.15	6.3476	6.6186
258.15	7.2898	7.5728	258.15	7.3450	7.628
253.15	8.4955	8.7903	253.15	8.5365	8.8302
248.15	9.9955	10.302	248.15	10.065	10.37
243.15	11.986	12.305	243.15	11.993	12.308
238.15	14.474	14.801	238.15	14.462	14.783
233.15	17.695	18.025	233.15	17.671	17.993
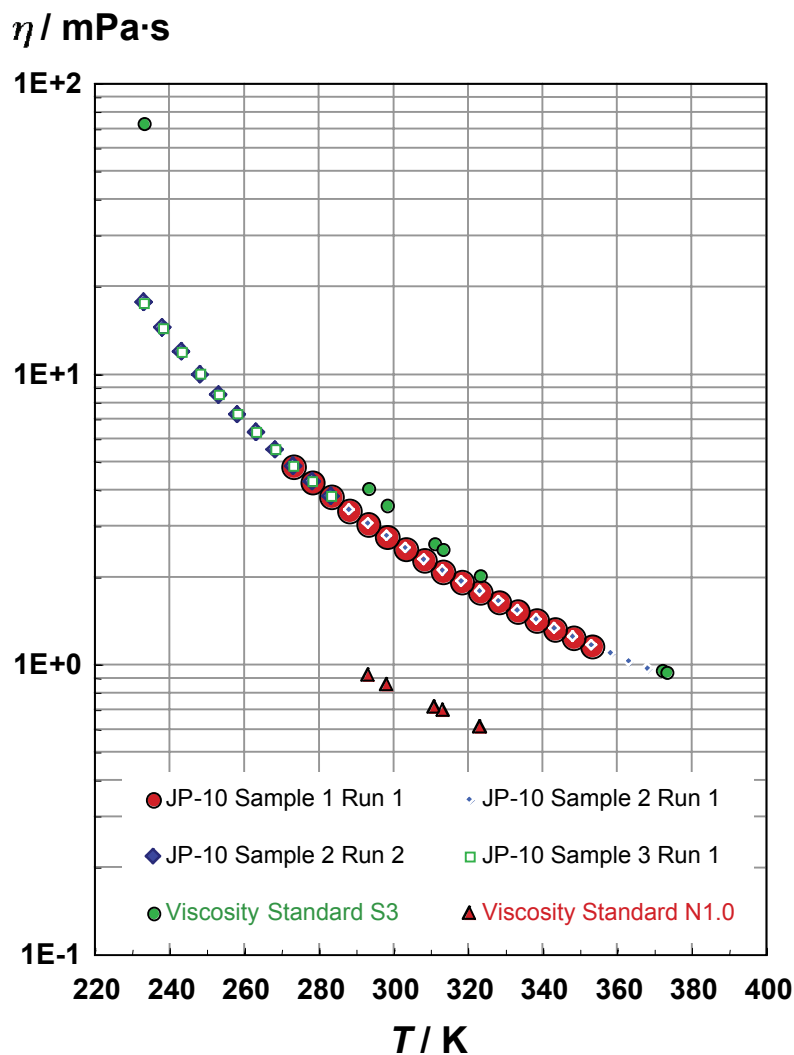
Figure 12. Absolute viscosities of JP-10 and of certified viscosity standard calibrating liquids S3 and N1.0 measured in the Stabinger viscodensimeter SVM 3000.

The percent deviations of the measured viscosities of the calibrating standards relative to the certified reference values are shown in Figure 13. The measured values for calibrating standard N1.0 deviate systematically between −10.8 % and −8.7 % from the certified reference values. These deviations are clearly beyond the uncertainty of the viscometer as quoted by the manufacturer (0.35 %). They are consistent with our earlier performance validations and experiences of other users of the Stabinger viscodensimeter, which indicate that the manufacturer quoted uncertainty is reached only in a viscosity range from 1 mPa·s to 1 Pa·s. The viscosities of JP-10 are within this range. Note that the viscosity of calibrating standard N1.0 is about three times lower than that of JP-10. Figure 13 shows that the percent deviations of the measured viscosities of calibrating standard S3 agree with the certified reference values within 0.42 %. This deviation is consistent with the combined manufacturer quoted uncertainty of the viscometer and the uncertainty of the certified reference values. Since the viscosity of calibrating

standard S3 matches that of JP-10 more closely, and based on the accumulated experience of this laboratory, the actual uncertainty of the viscosity measurements of JP-10 is estimated at ±1 %.
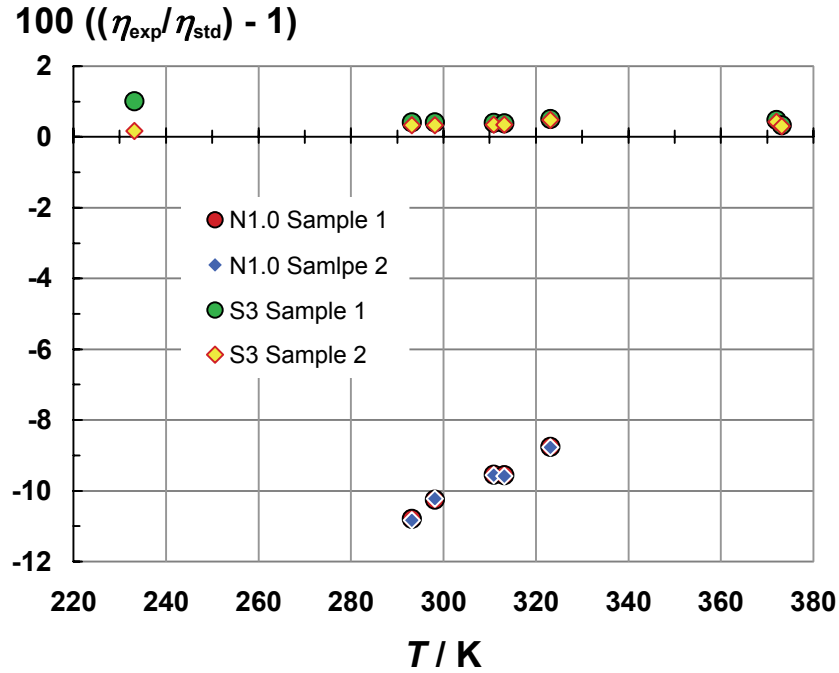
Figure 13. Percent deviations of the measured viscosities of the calibrating standards relative to the certified reference values.

Viscosity correlation

To facilitate the practical application of the measured viscosities, their temperature dependence was also correlated in this work. The curvature of the logarithmically scaled experimental viscosity data in Figure 12 indicates that simple exponential terms such as the Arrhenius *ansatz* are insufficient to represent the data within their experimental uncertainty. The Vogel-Tammann-Fulcher (VTF) equation is applicable over wider ranges of temperature but was also found inadequate for the wide-ranging JP-10 viscosity measured here. Adding two temperature terms to the VTF equation yielded a representation of the viscosity data well within their experimental uncertainty. The reduced absolute viscosity is expressed as a function of the reduced absolute temperature according to

$$\frac{\eta}{\eta_0} = \exp\left(\frac{\beta_1}{T_r + \beta_2} + \beta_3 T_r + \beta_4 T_r^2\right) \tag{7}$$

where $\eta_0 = 1$ mPa·s is a dimensional reducing factor and $T_r = T / (273.15 \text{ K})$ is the reduced absolute temperature. The values of the adjustable parameters β_1 to β_4 were determined by nonlinear least squares regression. They are listed with their standard deviations in Table 9. The

experimental viscosity data are represented by eq. (7) with a maximum negative deviation of −0.62 % and a maximum positive deviation of 0.63 %. These deviations are within the estimated uncertainty of the data of 1 %.

Table 9. Parameter values and associated standard deviations of the viscosity correlation eq. (7).

i	Parameter β_i	Standard deviation s_i
1	1.82400	0.0099
2	−0.430094	0.0013
3	−1.99450	0.025
4	0.370442	0.014

The percent deviations of the experimental viscosity data from the correlation are illustrated in Figure 14. The curvature of the deviations at either end of the temperature range should caution users of eq. (7) not to extrapolate the correlation beyond the temperature limits. The graph gives also an impression of the repeatability of the viscosity measurements in the Stabinger viscodensimeter with different samples from the same stock.
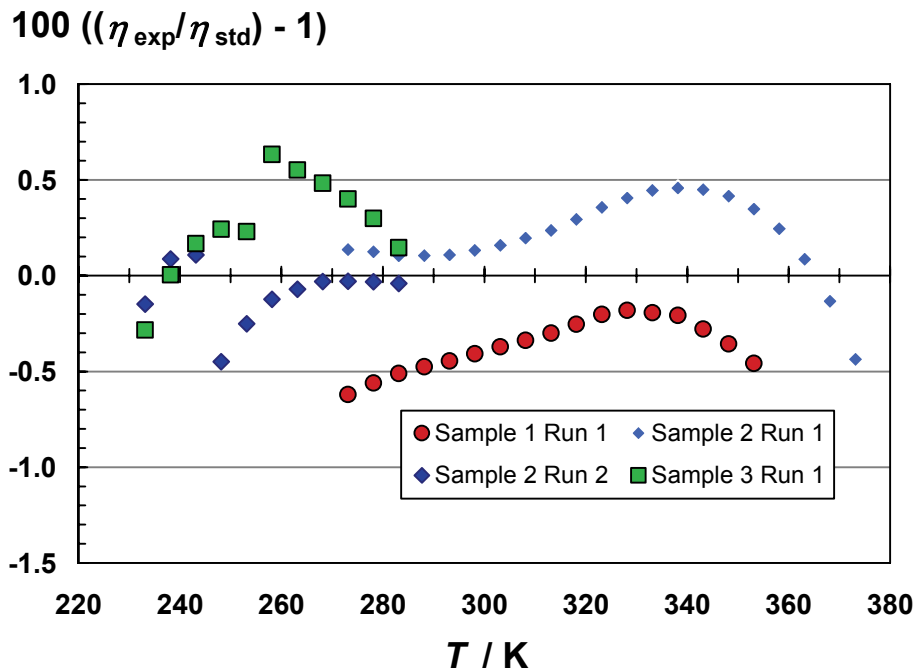
Figure 14. Percent deviations of the measured viscosities of JP-10 relative to the correlation, eq. (7).

Sound Speed Measurements and Derived Adiabatic Compressibilities for JP-10

The speed of sound in JP-10 was measured in the Sound Speed Analyzer DSA 5000 between 278.15 K and 343.15 K. The results are tabulated in Table 10 and illustrated in Figure 15. Table 10 includes also derived values of the adiabatic compressibility $\kappa_s = -(\partial V/\partial p)_s/V = 1/(\rho w^2)$. These are illustrated in Figure 16.
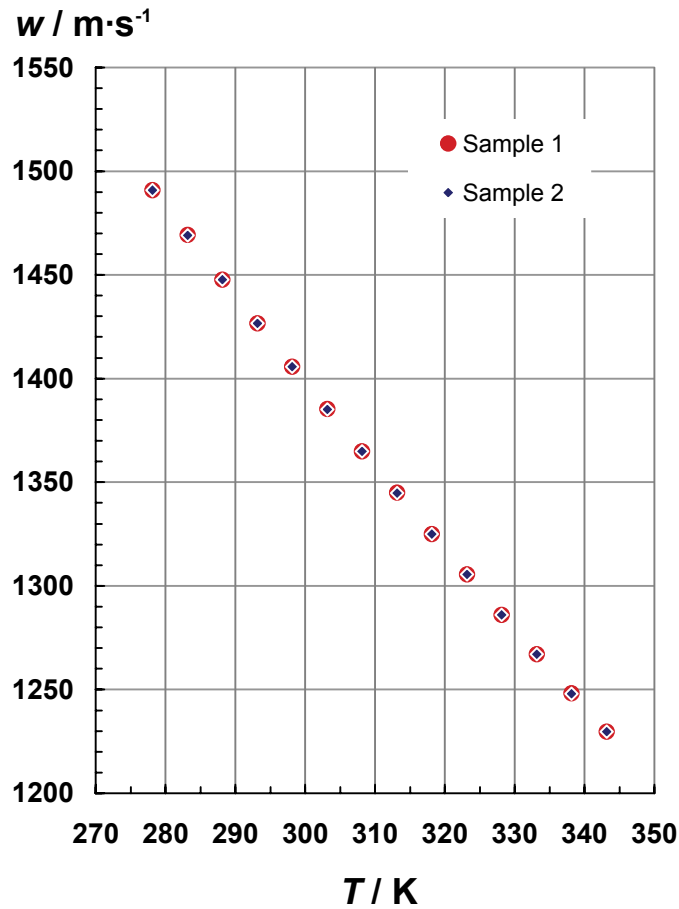
Figure 15. Speed of sound in JP-10 measured in the sound speed analyzer DSA 5000.

Table 10. Speeds of Sound and derived Adiabatic Compressibilities of JP-10 measured in the Sound Speed Analyzer DSA 5000. The ambient pressure during the measurements was 84 kPa.

Temperature T	Speed of sound w	Adiabatic compressibility κ_s	Temperature T	Speed of sound w	Adiabatic compressibility κ_s
K	m·s^{-1}	GPa^{-1}	K	m·s^{-1}	GPa^{-1}
	Run 1			*Run 2*	
343.152	1229.62	0.737932	343.150	1229.59	0.737971
338.151	1248.15	0.713035	338.150	1248.11	0.713083
333.150	1267.03	0.688918	333.150	1266.98	0.688974
328.151	1286.14	0.665692	328.151	1286.09	0.665748
323.149	1305.47	0.643335	323.151	1305.43	0.643377
318.150	1325.04	0.621793	318.150	1325.00	0.621832
313.151	1344.85	0.601036	313.152	1344.79	0.601093
308.151	1364.90	0.581036	308.151	1364.83	0.581098
303.152	1385.21	0.561743	303.151	1385.16	0.561787
298.152	1405.80	0.543117	298.151	1405.74	0.543167
293.151	1426.63	0.525167	293.152	1426.58	0.525206
288.151	1447.73	0.507846	288.151	1447.66	0.507898
283.151	1469.17	0.491087	283.150	1469.13	0.491116
278.147	1490.93	0.474888	278.143	1490.95	0.474877
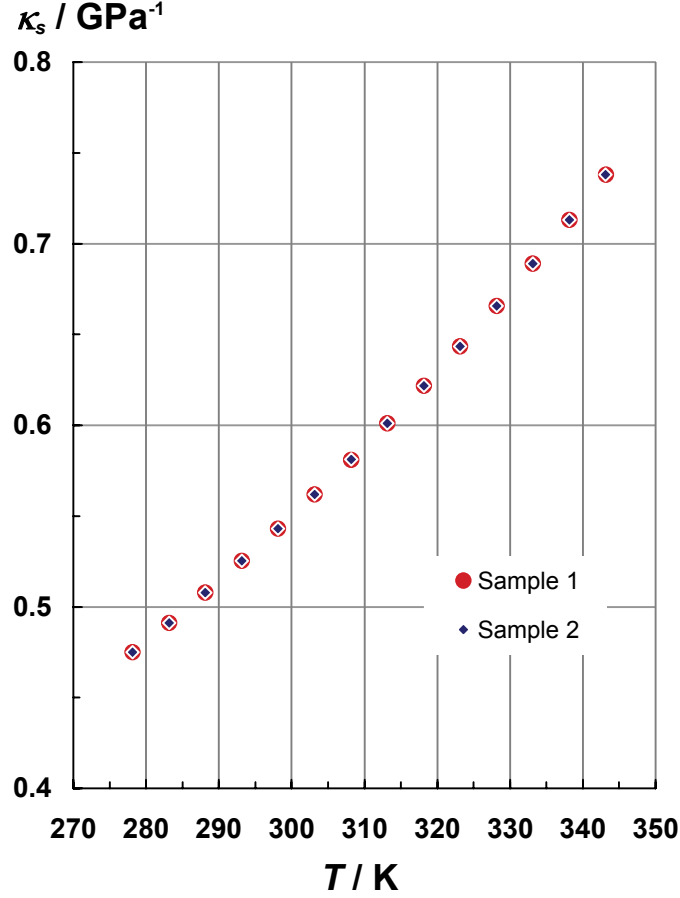
Figure 16. Adiabatic compressibilities of JP-10 derived from measurements in the sound speed analyzer DSA 5000.

Thermal Conductivity of JP-10

Transient hot-wire measurements of the thermal conductivity of the JP-10 liquid sample were made along 11 isotherms at temperatures from 300 to 500 K with pressures up to 30 MPa. The transient hot-wire instrument has been described in detail elsewhere[15]. The measurement cell is designed to closely approximate transient heating from a line source into an infinite fluid medium. The ideal (line source) temperature rise ΔT_{id} is given by

$$\Delta T_{id} = \frac{q}{4\pi\lambda}\left[\ln(t) + \ln\left(\frac{4a}{r_0^2 C}\right)\right] = \Delta T_w + \sum_{i=1}^{10}\delta T_i, \tag{8}$$

where q is the power applied per unit length, λ is the thermal conductivity of the fluid, t is the elapsed time, $a = \lambda/\rho C_p$ is the thermal diffusivity of the fluid, ρ is the density of the fluid, C_p is the isobaric specific heat capacity of the fluid, r_0 is the radius of the hot wire, $C = 1.781...$ is the exponential of Euler's constant, ΔT_w is the measured temperature rise of the wire, and δT_i are corrections to account for deviations from ideal line-source conduction [15,16]. The only significant

28

correction for the JP-10 measurements is for the finite wire dimensions. A plot of ideal temperature rise versus log of elapsed time should be linear, such that thermal conductivity can be found from the slope and thermal diffusivity can be found from the intercept of a linear fit to the data.

At time zero, a fixed voltage is applied to heat the small diameter wire that is immersed in the fluid of interest. The wire is used as an electrical heat source while its resistance increase allows determination of the transient temperature rise as a function of elapsed time. A single anodized tantalum wire of 25 μm diameter and 10 cm length was used for the measurements. Short experiment times (nominally 1 s) and small temperature rises (nominally 1 to 4 K) are selected to eliminate heat transfer by free convection. Experiments at several different heating powers (and temperature rises) provide verification that free convection is not significant. Heat transfer due to thermal radiation is more difficult to detect and correct when the fluid can absorb and re-emit infrared radiation, as does JP-10. Thermal radiation heat transfer will increase roughly in proportion to the absolute temperature cubed and can be characterized from an increase in the apparent thermal conductivity as experiment time increases since radiation emission from the fluid increases as the thermal wave diffuses outward [16]. Measurements of toluene liquid made prior to the JP-10 measurements verified that the apparatus was performing correctly. The toluene verification measurements at 300 K and 320 K agreed with IUPAC recommendations within 1 % at a 95 % confidence interval.

The results of 683 transient hot-wire measurements are given in Appendix 1 and shown in Figure 17 at temperatures from 300 K to 500 K. Each experiment is characterized by the initial cell temperature T_0 and the mean experiment temperature T_e. There are generally five experiments at each initial cell temperature to verify that convection was not significant, since convection depends strongly on the temperature rise ($\Delta T = T_e - T_0$). The conditions of the fluid during each measurement are given by the experimental temperature T_e, pressure p_e, and density ρ_e. The thermal conductivity without correction for thermal radiation is given by λ_e; the contribution of thermal radiation to the measured thermal conductivity is less than 0.5 % at the highest temperature of 500 K. The uncertainty of the measured thermal conductivity data is less than 1 % for temperatures from 300 to 500 K.
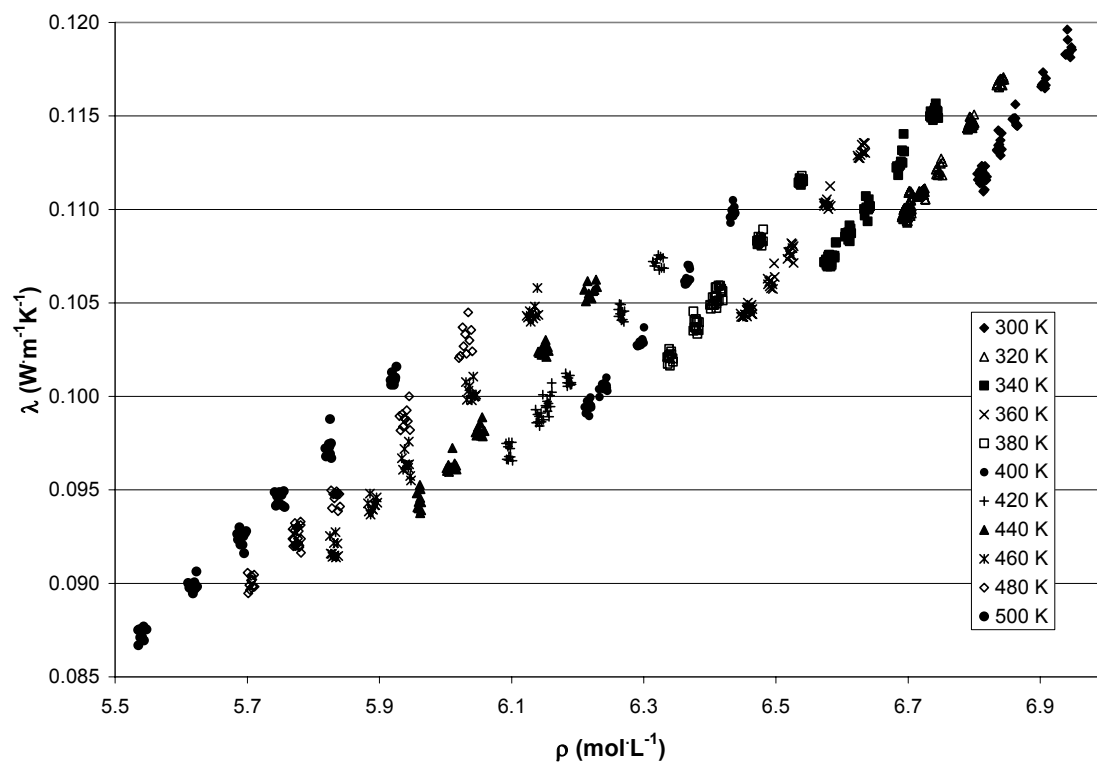
Figure 17. Thermal conductivity of JP-10 at pressures from 0.1 MPa to 30 MPa.

Distillation Curve for JP-10

One normally associates the distillation curve measurement with complex mixtures, such as crude oils, gasolines, and kerosenes. The distillation curve of what is nominally a pure fluid is really a measurement of a vapor pressure. Since several components were found in the sample of JP-10 that was used for all of the measurements discussed in this report, it was decided that the distillation curve would be instructive.

The distillation curve of JP-10 was measured with a developmental apparatus that incorporates several important improvements over previous approaches [17]. The main improvement has been the introduction of a composition channel, allowing on-the-fly sampling of distillate for a quantitative analysis. In addition, there have been improvements in temperature measurement and control, and in the liquid volume measurement.

The distillation curve that was measured for JP-10 is provided in Figure 18. This curve is presented as temperature (T_k, measured directly in the liquid) plotted against volume fraction. The temperatures were measured at an ambient atmospheric pressure of 84.06 kPa. These temperatures have been converted to what would have been measured at standard atmospheric pressure with the modified Sidney Young equation:

$$C_c = C(760 - P_a)(273 + T) , \qquad (9)$$

where C_c is the correction added to the observed temperature, C is a constant, Pa is the atmospheric pressure in mmHg, and T is the measured temperature in °C. In fact, the original Sidney Young equation specifies that C is dependent upon the average hydrocarbon chain length of the fluid, ranging from 0.000135 for a single carbon to 0.000119 for 8 carbons. A linear correlation of these factors can be used to predict a value for simple fluids. It should be noted that the Sidney Young equation may have significant limitations when applied to correct boiling point temperatures more than 5 kPa from standard atmospheric pressure [18].

It can be seen that this curve is indeed indicative of a single component fluid. Despite the seven identified components, the distillation properties of this fluid are best described as a vapor pressure, within a first approximation. The boiling temperature at 84.06 kPa was found to be 180.8 °C, with an uncertainty of 0.2 °C. When corrected to standard atmospheric pressure with the Sidney Young equation, a boiling temperature of 187.2 °C is obtained, also with an uncertainty of 0.2 °C. Note that 18 separate measurements are used to calculate these values; the final inflection point represents lift-out of the sensing thermocouple, and the end of a measurement.
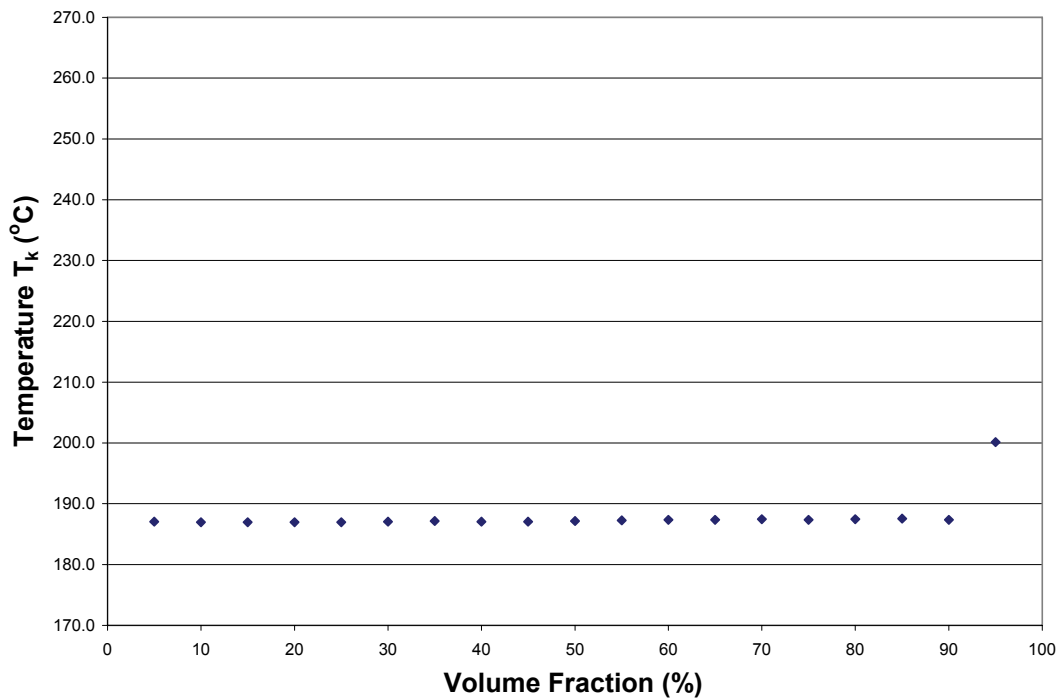
Figure 18. The distillation curve for JP-10, as received from Wright Laboratory. T_k represents the temperature measured directly in the liquid (the kettle) corrected with the Sidney Young equation. This curve is essentially the distillation curve of a pure fluid. Note that the inflection seen at the highest volume fraction is the result of the lift out of the measuring thermocouple, and is not part of the distillation curve proper.

Model Development for the Thermodynamic and Transport Properties of JP-10

In order to begin model development for the thermophysical properties of JP-10, we first collected data from the literature. The experimental data in the literature are very limited; a summary is presented in Table 11. There is no information on density, viscosity, heat capacity, sound speed, or thermal conductivity at pressures above the saturation boundary. The most comprehensive sets are those of Steele et al. [19] which provide the critical point, a vapor pressure curve, heat capacities and liquid densities at saturation conditions, and Moynihan et al. [20] which provides limited liquid density and viscosity data at atmospheric pressure. For this work it is therefore important to have NIST measurements of thermophysical properties to supplement the very limited information in the open literature.

Table 11. Summary of literature data on the thermophysical properties of JP-10.

Source	Summary of properties
Boyd et al., 1971 [21]	Vapor pressure correlating equation only ($358 \leq T(K) \leq 417$) c_p^0, 5 points ($200 \leq T(K) \leq 500$) c_p, 4 points ($329 \leq T(K) \leq 390$)
Moynihan et al., 1977 [22]	Correlating equations given for c_p, density and viscosity of the liquid at atmospheric pressure
Moynihan et al., 1978 [23]	Repeats information in Moynihan et al., 1977
Smith et al., 1978 [24]	c_p correlating equation only
Smith and Good, 1979 [25]	One experimental liquid density and c_p point (298 K)
Smith et al., 1980 [26]	c_p correlating equation only
Gammon and Smith, 1982 [27]	Two experimental liquid density points (288 K, 298 K)
Moynihan et al., 1982 [20]	Liquid density and viscosity at atmospheric pressure, 17 points for ($219 \leq T(K) \leq 322$)
Steele et al., 1989 [19]	Critical point, Vapor pressure, 23 points ($343 \leq T(K) \leq 507$) Saturated liquid density, 3 points ($690 \leq T(K) \leq 698$) Saturated vapor density, 4 points ($681 \leq T(K) \leq 698$) c_{sat}, 39 points ($300 \leq T(K) \leq 680$)
Chickos et al., 2002 [28]	c_p, 10 points ($193 \leq T(K) \leq 273$) Heat of vaporization, 1 point (298 K)
CRC, Inc., 2004 [29]	Provides graphical information only on liquid density at atmospheric pressure, kinematic viscosity at atmospheric pressure, surface tension, vapor pressure, specific heat and liquid thermal conductivity at atmospheric pressure, dielectric constant.

Thermodynamic Properties of JP-10

A fundamental equation of state for JP-10 has been developed, explicit in Helmholtz energy as a function of density and temperature. All single-phase thermodynamic properties can be calculated as derivatives of the Helmholtz energy. A preliminary equation of state for propane was used as the starting point for the equation of state developed here for JP-10. Unlike high accuracy equations, which generally use 20 to 50 fluid-specific terms to describe densities to the order of (0.01 to 0.1) %, the equation presented here has only 10 terms. For JP-10, there are not sufficient experimental data available to develop a high-accuracy fluid-specific model with 20 to 50 terms similar to that done in other work.

The extrapolation of the equation of state can be checked at low temperatures (as demonstrated by the curvature of the isobaric and isochoric heat capacities, and the speed of sound) and at high temperatures (as demonstrated by the ideal curves). In addition, the number of terms in the equation (10 terms for the real gas) was kept to a minimum, thus decreasing the correlation among terms and the possibility of over fitting. Although the smaller number of terms decreases the flexibility of the equation, and thus its ability to accurately represent a fluid's properties, its rigid shape becomes more applicable to substances with limited data, and thus becomes a tool to fill in gaps in the thermodynamic surface, a key feature in modeling fluids such as JP-10.

The critical temperature and pressure were taken from Steele et al. [19] Although Steele et al. reported a value for the critical density (2.092 mol/dm^3), this value appeared to be too low and was not used here, rather, the critical density was fitted simultaneously with the coefficients of the equation, resulting in a value of 2.16 mol/dm^3. Steele et al. did not actually measure the critical density, rather it was graphically selected by plotting a line through their seven critical region values of the saturated densities. The method used in this work to determine the critical density also uses these seven values, in additional to all of the other available data for JP-10, and is thus a more reliable technique for the critical density prediction. The values of the critical parameters reported below should be used for all property calculations from the equation of state.

T_c = 698 K
p_c = 3.733 MPa
ρ_c = 2.16 mol/dm^3

The equation of state, expressed in a fundamental form explicit in the Helmholtz energy, has become the most widely used method for calculating thermodynamic properties with high accuracy for many fluids. The independent variables in the functional form are density and temperature,

$$a(\rho,T) = a^0(\rho,T) + a^r(\rho,T) \quad , \tag{10}$$

where a is the Helmholtz energy, $a^0(\rho,T)$ is the ideal gas contribution to the Helmholtz energy, and $a^r(\rho,T)$ is the real fluid Helmholtz energy that results from intermolecular forces. All thermodynamic properties can be calculated as derivatives of the Helmholtz energy. For example, the pressure derived from this expression is

$$p = \rho^2 \left(\frac{\partial a}{\partial \rho} \right)_T .$$ (11)

In practical applications, the functional form used is the dimensionless Helmholtz energy, α, as a function of a dimensionless density and temperature. The form of this equation is

$$\frac{a(\rho, T)}{RT} = \alpha(\delta, \tau) = \alpha^0(\delta, \tau) + \alpha^r(\delta, \tau),$$ (12)

where $\delta = \rho / \rho_c$ and $\tau = T_c / T$. The Helmholtz energy of the ideal gas is given by

$$a^0 = h_0^0 + \int_{T_0}^{T} c_p^0 dT - RT - T \left[s_0^0 + \int_{T_0}^{T} \frac{c_p^0}{T} dT - R \ln \left(\frac{\rho T}{\rho_0 T_0} \right) \right],$$ (13)

where ρ_0 is the ideal gas density at T_0 and p_0 ($\rho_0 = p_0/T_0R$) and T_0 and p_0 are arbitrary constants. The ideal gas Helmholtz energy is given in a dimensionless form by

$$\alpha^0 = \frac{h_0^0 \tau}{RT_c} - \frac{s_0^0}{R} - 1 + \ln \frac{\delta \tau_0}{\delta_0 \tau} - \frac{\tau}{R} \int_{\tau_0}^{\tau} \frac{c_p^0}{\tau^2} d\tau + \frac{1}{R} \int_{\tau_0}^{\tau} \frac{c_p^0}{\tau} d\tau ,$$ (14)

where $\delta_0 = \rho_0 / \rho_c$ and $\tau_0 = T_c / T_0$.

The calculation of thermodynamic properties from the ideal gas Helmholtz energy requires an equation for the ideal gas heat capacity, c_p^0. These values can be obtained from heat capacity measurements extrapolated to zero pressure, gaseous speed of sound measurements, or calculations from statistical methods using spectroscopically determined frequencies. In this work, we fitted the following equation simultaneously with the other parameters in the real gas part of the equation.

$$\frac{c_p^0}{R} = c_0 + c_1 T^{0.85} + c_2 \left(\frac{c_3}{T} \right)^2 \frac{\exp(c_3/T)}{\left[\exp(c_3/T) - 1 \right]^2} ,$$ (15)

Here, the molar gas constant, R, is 8.314472 J·mol^{-1}·K^{-1} and the values of the coefficients are c_0 = 3.3218, c_1 = 0.07975, c_2 = 27.6975, and c_3 = 1470. The values of c_p^0 in Boyd et al. [21] supplemented at temperatures over 600 K with values for a similar compound, adamantine [21] were used in the fitting. The ideal gas Helmholtz energy equation, derived from eqs. (14) and (15), is

$$\alpha^0 = a_1 + a_2 \tau + \ln \delta + (c_0 - 1) \ln \tau - \frac{c_1 T_c^{0.85}}{0.85(1.85)} \tau^{-0.85} + c_2 \ln\left[1 - \exp(-c_3 \tau / T_c) \right],$$ (16)

where a_1 and a_2 are arbitrary, and are conventionally chosen by the definition of the reference state for enthalpy and entropy.

The common functional form used for the Helmholtz energy equation of state is

$$\alpha^r(\delta,\tau) = \sum_k N_k \delta^{i_k} \tau^{j_k} + \sum_k N_k \delta^{i_k} \tau^{j_k} \exp\left(-\delta^{l_k}\right), \tag{17}$$

where each summation typically contains 4 to 20 terms and where the index k points to each individual term. The functional form used here is:

$$\begin{aligned}
\alpha^r(\delta,\tau) = & \; n_1\delta\tau^{0.2} + n_2\delta\tau^{1.15} + n_3\delta^2\tau^{1.42} + n_4\delta^2\tau^{1.65} + n_5\delta^4\tau \\
& + n_6\delta^3\tau^{2.0}\exp^{-\delta} + n_7\delta^3\tau^{1.69}\exp^{-\delta} + n_8\delta^6\tau^{0.95}\exp^{-\delta} \;, \\
& + n_9\delta^6\tau^{1.72}\exp^{-\delta} + n_{10}\delta^4\tau^{2.5}\exp^{-\delta^2}
\end{aligned} \tag{18}$$

where the coefficients n_k of the residual part of the equation of state are given in the table below.

Table 12. Coefficients of the equation of state.

k	n_k
1	1.64044
2	−2.75277
3	−1.04100
4	0.909461
5	0.0396564
6	−0.429241
7	1.21962
8	0.0609974
9	−0.0798114
10	−0.0439556

The functions used for calculating pressure (p), compressibility factor (Z), internal energy (u), enthalpy (h), entropy (s), Gibbs energy (g), isochoric heat capacity (c_v), isobaric heat capacity (c_p), and the speed of sound (w) are:

$$Z = \frac{p}{\rho RT} = 1 + \delta\left(\frac{\partial\alpha^r}{\partial\delta}\right)_\tau \tag{19}$$

$$\frac{u}{RT} = \tau\left[\left(\frac{\partial\alpha^0}{\partial\tau}\right)_\delta + \left(\frac{\partial\alpha^r}{\partial\tau}\right)_\delta\right] \tag{20}$$

$$\frac{h}{RT} = \tau\left[\left(\frac{\partial\alpha^0}{\partial\tau}\right)_\delta + \left(\frac{\partial\alpha^r}{\partial\tau}\right)_\delta\right] + \delta\left(\frac{\partial\alpha^r}{\partial\delta}\right)_\tau + 1 \tag{21}$$

$$\frac{s}{R} = \tau\left[\left(\frac{\partial\alpha^0}{\partial\tau}\right)_\delta + \left(\frac{\partial\alpha^r}{\partial\tau}\right)_\delta\right] - \alpha^0 - \alpha^r \tag{22}$$

$$\frac{g}{RT} = 1 + \alpha^0 + \alpha^r + \delta\left(\frac{\partial\alpha^r}{\partial\delta}\right)_\tau \tag{23}$$

$$\frac{c_v}{R} = -\tau^2\left[\left(\frac{\partial^2\alpha^0}{\partial\tau^2}\right)_\delta + \left(\frac{\partial^2\alpha^r}{\partial\tau^2}\right)_\delta\right] \tag{24}$$

$$\frac{c_p}{R} = \frac{c_v}{R} + \frac{\left[1 + \delta\left(\frac{\partial\alpha^r}{\partial\delta}\right)_\tau - \delta\tau\left(\frac{\partial^2\alpha^r}{\partial\delta\partial\tau}\right)\right]^2}{\left[1 + 2\delta\left(\frac{\partial\alpha^r}{\partial\delta}\right)_\tau + \delta^2\left(\frac{\partial^2\alpha^r}{\partial\delta^2}\right)_\tau\right]} \tag{25}$$

$$\frac{w^2 M}{RT} = 1 + 2\delta\left(\frac{\partial\alpha^r}{\partial\delta}\right)_\tau + \delta^2\left(\frac{\partial^2\alpha^r}{\partial\delta^2}\right)_\tau - \frac{\left[1 + \delta\left(\frac{\partial\alpha^r}{\partial\delta}\right)_\tau - \delta\tau\frac{\partial^2\alpha^r}{\partial\delta\partial\tau}\right]^2}{\tau^2\left[\left(\frac{\partial^2\alpha^0}{\partial\tau^2}\right)_\delta + \left(\frac{\partial^2\alpha^r}{\partial\tau^2}\right)_\delta\right]} \cdot \tag{26}$$

The derivatives of the ideal gas Helmholtz energy and the residual Helmholtz energy required by the equations for the thermodynamic properties are given in Lemmon et al. [30]

In the development of equations of state, various data types are useful in evaluating other types of data. Since one equation is used to represent multiple properties, the accuracy of one property can influence the behavior of another. In particular, the availability of heat capacity data is fundamental in equation of state development. Without it, equations can inadvertently give negative heat capacities at low temperatures or show unrealistic curvature in certain areas of the thermodynamic surface. For JP-10, the differences in the heat capacities among the various data sets is large, and new measurements will help access the uncertainties in the data sets. Although the quantity of heat capacity data for a fluid may be limited, even a few values in the liquid phase can often be sufficient to tie down the equation of state when working with a fixed functional form. This can be confirmed by plotting various constant property lines over the surface of state, and by comparing the slopes of such lines to expected behavior. The extrapolation behavior of the functional form used here at low and high temperatures, pressures, and densities gives confidence in the equation of state in the absence of highly accurate experimental data over some areas of the thermodynamic surface.

Nonlinear fitting techniques were used to fit the coefficients of the equation. The selected data used in fitting were a subset of the available database determined by the correlator to be representative of the most accurate values measured. The nonlinear algorithm adjusted the coefficients and temperature exponents of the equation of state to reduce the overall sum of squares of the deviations of calculated properties from the input data. Each data point was individually weighted according to type, region, and uncertainty. Additionally, the values of the first and second derivatives of pressure with respect to density at the critical point were forced to be near zero at the selected critical point. The final set of coefficients represented not only the fitted data, but also the consistent data available for JP-10.

Figure 19 shows deviations in density from about 200 to 350 K (the range of the experimental data). Comparisons with the equation of state to the data measured in this work and the data of Moynihan et al. [20,23] are very consistent and are generally within 0.1 %. The equation of state was fitted to the data measured in this work and is generally within 0.04 %. There are no experimental measurements above atmospheric pressure, above 400 K, or in the vapor phase, except for seven saturated liquid or vapor points from Steele et al. [19] in the critical region. The deviations are much larger than those at lower temperatures, but this is to be expected due to the nature of the critical region. Figure 20 shows these seven points and their proximity to the calculated saturation line from the equation of state. The data point with the highest density may be in error, and was not used in fitting. One of the data points was reported by Steele et al. to be in the liquid phase. However, with the change of critical density in this work, that point is actually in the vapor phase.
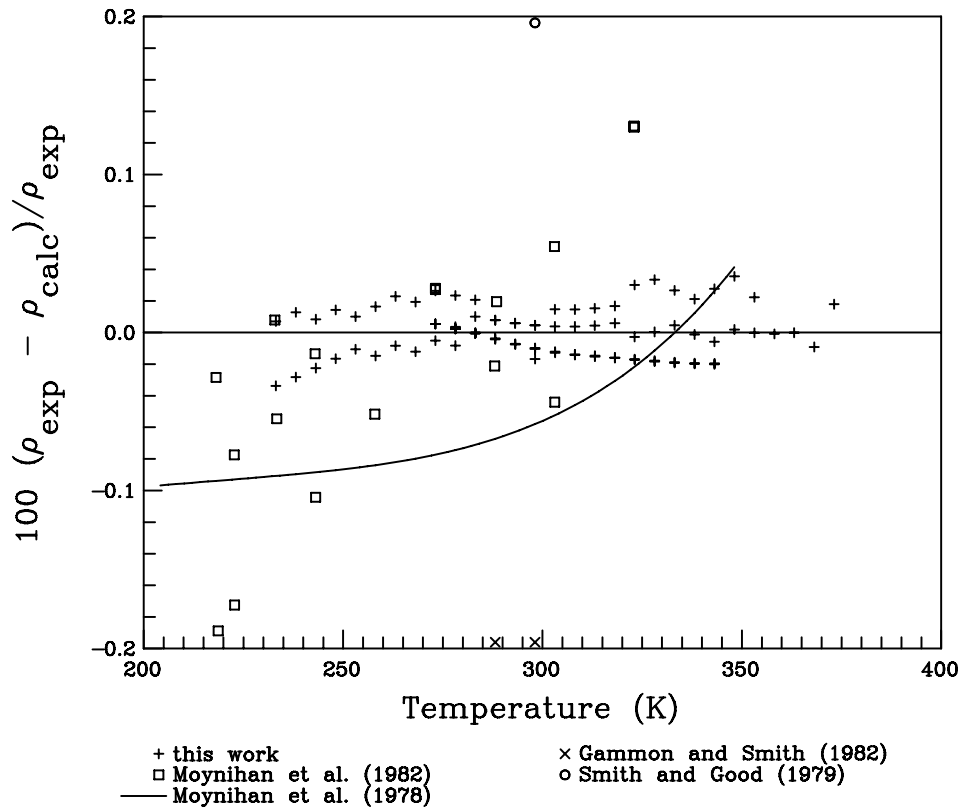
Figure 19. Density deviations of available experimental data from the model.
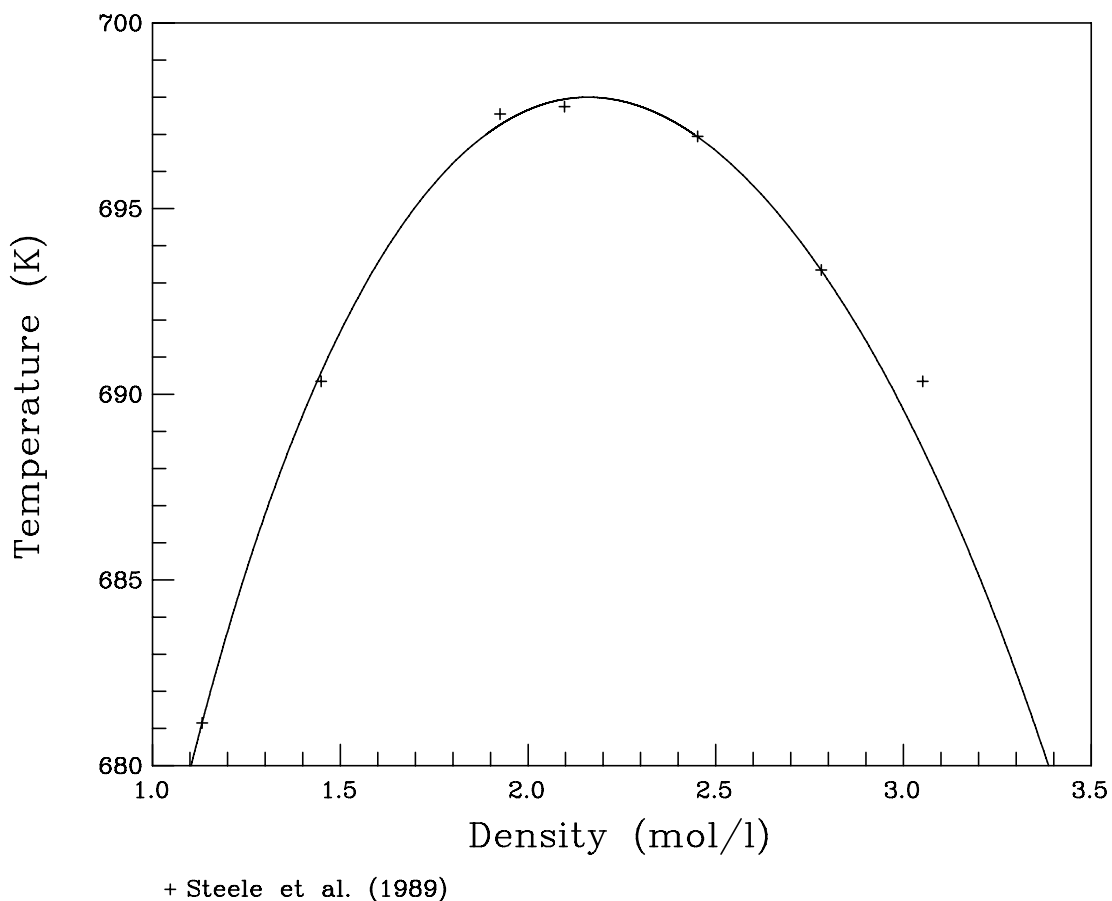
Figure 20. Saturation boundary of JP-10.

Figure 21 shows comparisons of the equation of state with vapor pressure measurements. There is a definite need for additional measurements due to the large scatter between the data sets. The equation was fit to the boiling point determined at 84.06 kPa, measured in this work. The values from Steele et al. [19] vary substantially from this, and are 3 to 6% off from the equation of state. Likewise the equation of Boyd et al.[21] differs by –2 to –10 %. The deviation of the vapor pressure point measured in this work is less than 0.1 %, as is the deviation of the only available heat of vaporization point of Chickos et al.[28]
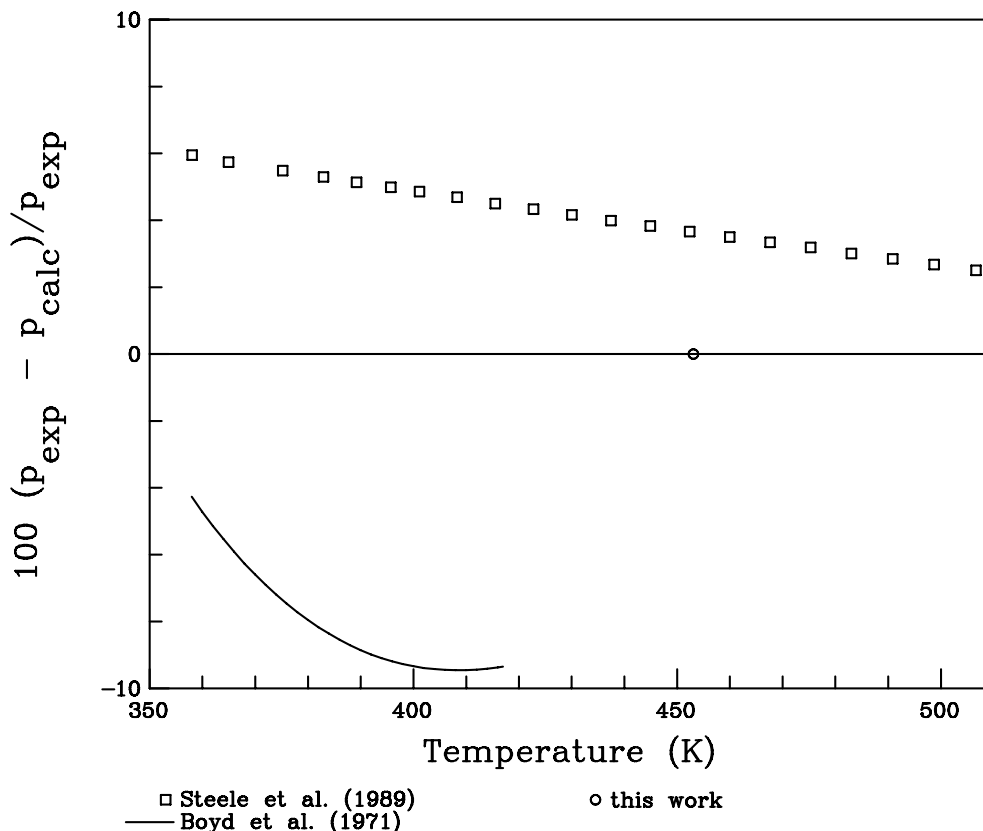
Figure 21. Deviations of vapor pressure for JP-10.

Figure 22 shows comparisons of the ideal gas heat capacity to the values given by Boyd et al. [21] The equation differs from the five points for JP-10 given by Boyd et al. by up to 0.4 %. For the high temperature points taken for the fluid adamantane, differences are similar, but rise to 0.8 % at 1000 K. Figure 23 shows the large scatter between the equation of state and other data sets for the isobaric and saturation heat capacities available for JP-10. The data of Chickos et al. [28] and the equation of Moynihan et al. [23] are about 5 % below the equation of state. The data of Steele et al. [19] and Boyd et al. [21] are about 5 % above the equation of state. The 1980 data from Smith et al. [19] compare the best with the equation, but the 1978 data from Smith et al. [24] show the largest deviations. Additional measurements of either the isobaric heat capacity or the isochoric heat capacity are needed to decrease the uncertainties in the equation of state for the heat capacity. There is only one set of measurements of the speed of sound for JP-10, measured as part of this work. The equation shows deviations of less than 0.04 %, as shown in Figure 24. Additional independent measurements of the speed of sound would help determine the total uncertainty of these data and of the equation of state.

41
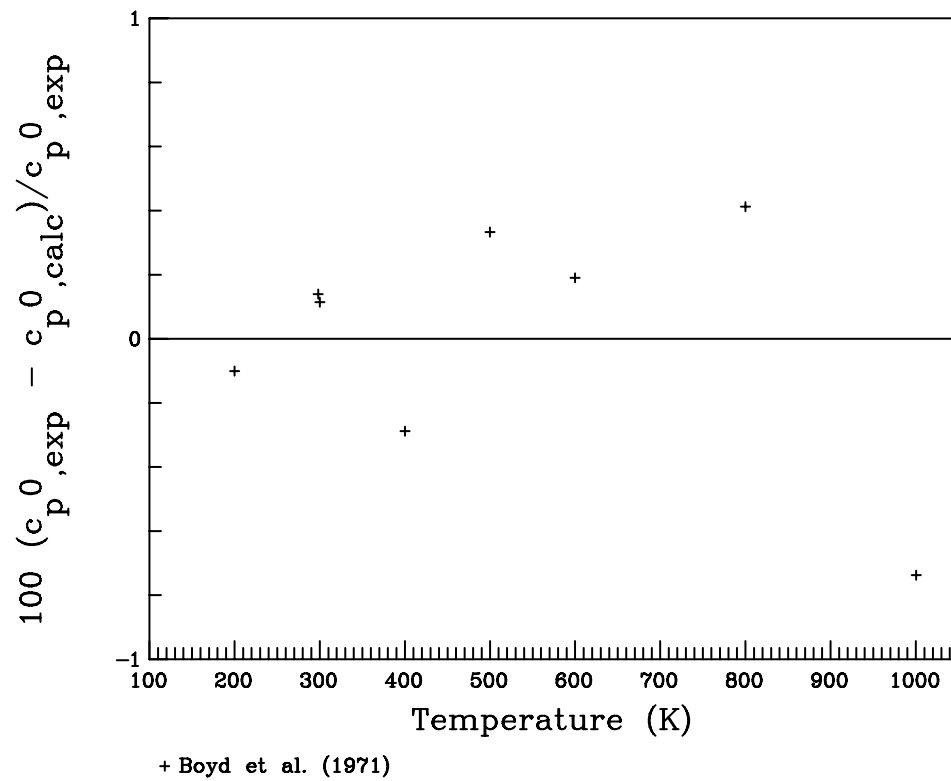
Figure 22. Deviations of the ideal gas heat capacity of JP-10.

Figure 23. Deviations of the isobaric and saturation heat capacities of JP-10.
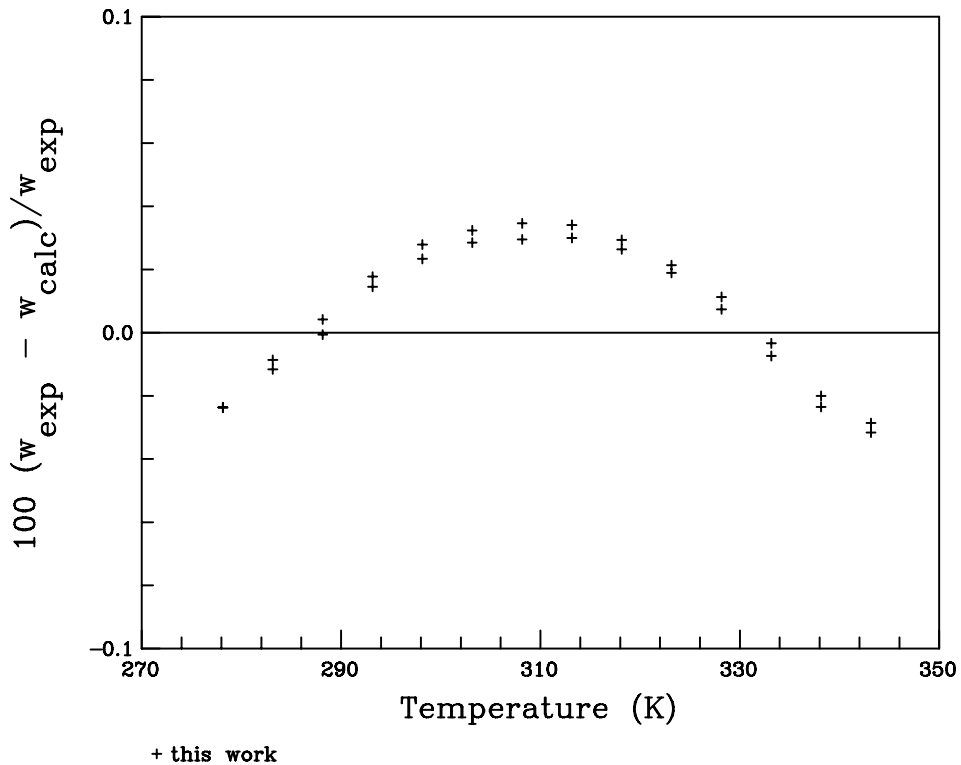
Figure 24. Deviations of the speed of sound for JP-10.

The uncertainties of properties calculated using the new equations are 0.1 % in density and in the speed of sound for the liquid phase at temperatures below 400 K and at pressures below 0.2 MPa. Elsewhere the uncertainty in density rises to 1 % or more; experimental data are needed to validate this estimate. The uncertainties are 5 % in heat capacities and 2 % in vapor pressure (where all of the uncertainties for the equation of state can be considered as estimates of a combined expanded uncertainty with a coverage factor of 2). Deviations in the critical region are higher for all properties.

Transport Properties of JP-10

Viscosity Model

In this work, we apply the extended corresponding states (ECS) viscosity model as described in Ref. [31], where the viscosity of a pure fluid is a sum of a dilute gas and a residual contribution, and the corresponding states principle applies only to the residual contribution [32],

$$\eta(T,\rho) = \eta^*(T) + \Delta\eta(T,\rho) = \eta^*(T) + \Delta\eta_0(T_0,\rho_0)F_\eta(T,\rho), \qquad (27)$$

where the superscript * denotes a dilute gas value, and the subscript 0 denotes a reference fluid value. In this work we selected propane as a reference fluid, and use the formulations given in references [33-35] for the equation of state, viscosity, and thermal conductivity. The viscosity of the reference fluid is evaluated at a conformal temperature and density T_0 and ρ_0 given by

$$T_0 = T/f \quad \text{and} \qquad (28)$$

$$\rho_0 = \rho h. \qquad (29)$$

The quantities f and h are called equivalent substance reducing ratios, and relate the reference fluid to the fluid of interest using a ratio of critical parameters (denoted by the subscript c) and functions of temperature and density known as shape functions θ and Φ,

$$f = \frac{T_c}{T_{c0}}\theta \quad \text{and} \qquad (30)$$

$$h = \frac{\rho_{c0}}{\rho_c}\phi. \qquad (31)$$

The shape factors can be considered functions of both temperature and density. For small, nonpolar, almost-spherical molecules they are nearly unity and can be thought of as functions to compensate for deviations from a spherical shape. In this work, we use a form of the "exact" shape factor method [36].

The dilute gas viscosity in eq. (1) is found by Chapman-Enskog theory

$$\eta^*(T) = \frac{5\sqrt{mk_BT}}{16\pi\sigma^2\Omega^{(2,2)}}, \qquad (32)$$

where the dilute gas viscosity is η^*, m is the molecular mass, k_B is the Boltzmann constant, and T is the absolute temperature. We will further assume that a Lennard-Jones 12-6 potential applies, and use the Lennard-Jones collision diameter for σ.   Neufeld et al. [37] gave the following empirical correlation for the calculation of the collision integral $\Omega^{(2,2)}$

$$\Omega^{(2,2)} = 1.16145(T^*)^{-0.14874} + 0.52487e^{-0.77320T^*} + 2.16178e^{-2.43787T^*}, \qquad (33)$$

with the dimensionless temperature $T^* = k_BT/\varepsilon$, and ε the minimum of the Lennard-Jones pair-potential energy. The range of validity of this empirical correlation is $0.3 < T^* < 100$, and we have used the truncated form that does not include a sinusoidal term.

The factor F_η in eq. (27) is found from the expression

$$F_\eta = f^{1/2}h^{-2/3}\left[\frac{M}{M_0}\right]^{1/2}, \tag{34}$$

where M is the molar mass of the fluid and M_0 is the molar mass of the reference fluid. In order to improve the model, experimental viscosity data are used to determine an empirical correction factor, where one evaluates eq. (27) at $\rho_{0,v}$ instead of ρ_0, with

$$\rho_{0,v}(T,\rho) = \rho_0(T,\rho)\psi(\rho_r), \tag{35}$$

and ψ is a polynomial in reduced density $\rho_r = \rho/\rho_c$ of the form

$$\psi(\rho_r) = c_0 + c_1\rho_r + c_2\rho_r^2, \tag{36}$$

where the coefficients c_0, c_1 and c_2 are constants found from fitting the experimental viscosity data. We fit the experimental viscosity data from NIST determined in this work and obtained $c_0 = 1.38384$, $c_1 = -0.216585$ and $c_2 = 0.037507$. In addition, we used Lennard-Jones potential parameters $k_bT/\varepsilon = 554.3$ and $\sigma = 0.6325$ nm, estimated using the method of Chung [38]. Figure 25 gives comparisons with the experimental viscosity data. At present, all of the data are at atmospheric pressure. In the liquid phase, we estimate the uncertainty of the correlation to be approximately 2 %. The model is capable of predicting values at pressures above the saturation boundary, but data are not available for comparison. However, based on the behavior of this model with similar fluids, we estimate the uncertainty in the liquid phase at pressures to 10 MPa to be less than 5 %.
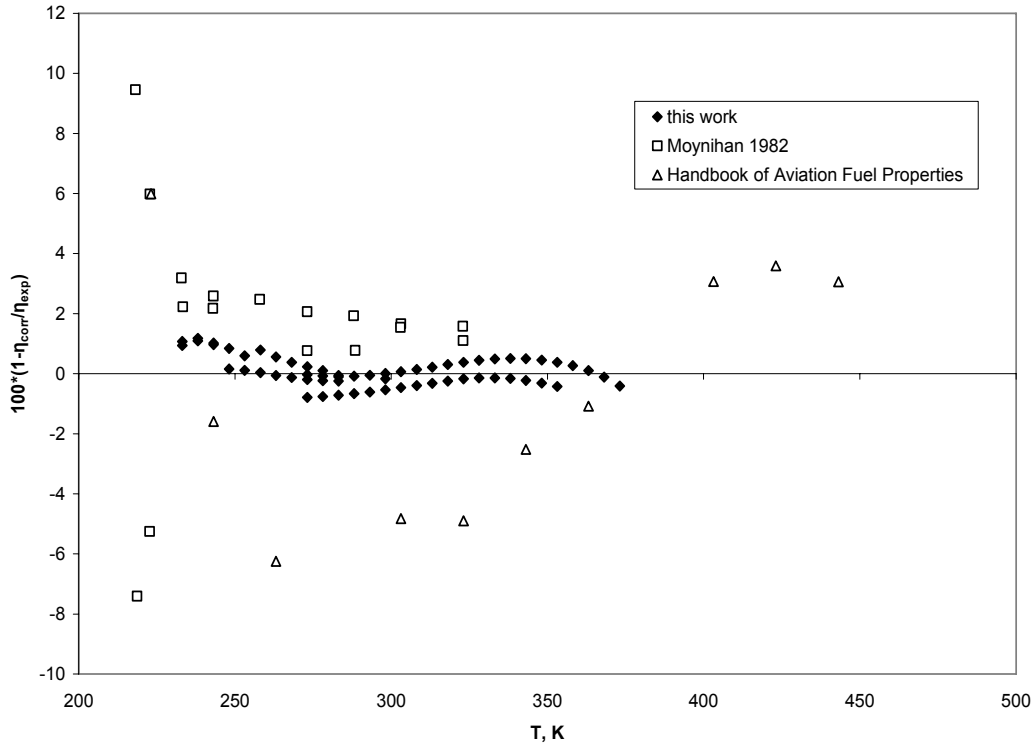
Figure 25. Deviations of viscosity of JP-10

Thermal Conductivity Model

We start with the procedure of Ely and Hanley [39] and represent the thermal conductivity of a fluid as the sum of translational (from collisions between molecules) and internal (due to internal motions of the molecule) modes of energy transfer,

$$\lambda(T,\rho) = \lambda^{int}(T) + \lambda^{trans}(T,\rho). \tag{37}$$

We use an Eucken correlation for the internal contribution

$$\lambda^{int}(T) = \frac{f_{int}\eta^*}{M}\left[c_p^* - \frac{5}{2}R\right], \tag{38}$$

where c_p^* is the ideal gas heat capacity in J/(mol·K), R is the molar gas constant [40], 8.314 472 J/(mol·K), η^* is the dilute-gas viscosity in μPa·s as given in eq. (32), f_{int} is set to $1.32 \cdot 10^{-3}$, and λ is in W/(m·K). If sufficient dilute-gas thermal conductivity data are available, f_{int} may be fit to a polynomial in temperature; however no data were available to do this so we have retained f_{int} as a constant.

The translational contribution may be further divided into a dilute-gas contribution (denoted here by a superscript $*$) that is a function only of temperature, a residual contribution, and a critical enhancement,

$$\lambda^{trans}(T,\rho) = \lambda^*(T) + \lambda^r(T,\rho) + \lambda^{crit}(T,\rho). \tag{39}$$

For the dilute-gas translational contribution (in W/(m·K)) we use

$$\lambda^*(T) = \frac{15 \cdot 10^{-3} R \eta^*}{4M}. \tag{40}$$

The residual contribution is found using extended corresponding states:

$$\lambda^r(T,\rho) = \lambda_0^r(T_0,\rho_0)F_\lambda, \text{ with} \tag{41}$$

$$F_\lambda = f^{1/2} h^{-2/3} \left[\frac{M_0}{M} \right]^{1/2}. \tag{42}$$

In order to improve the representation of the thermal conductivity, an empirical correction factor may be used if there are experimental thermal conductivity data available. We then evaluate eq. (41) at $\rho_{0,k}$ instead of ρ_0, where

$$\rho_{0,k}(T,\rho) = \rho_0(T,\rho)\chi(\rho_r), \tag{43}$$

and χ is a polynomial in reduced density $\rho_r = \rho/\rho_c$ of the form

$$\chi(\rho_r) = \sum_{k=0}^{n} b_k \rho_r^k, \tag{44}$$

where the coefficients b_k are found from fitting the experimental thermal conductivity data. We fit the experimental thermal conductivity data obtained as part of this work and obtained $b_0 = 1.11831$ and $b_1 = -0.0157596$.

We treat the final contribution, the critical enhancement, with a simplified crossover model developed by Olchowy and Sengers [41],

$$\lambda^{crit}(T,\rho) = \frac{\rho c_p R_0 k_B T}{6\pi\eta\xi}(\Omega - \Omega_0), \tag{45}$$

where the heat capacity at constant pressure, $c_p(T,\rho)$, is obtained from the equation of state, $R_0 = 1.03$ is a universal constant, and the viscosity, $\eta(T,\rho)$, is from the method described earlier. The crossover functions Ω and Ω_0 are determined by

$$\Omega = \frac{2}{\pi}\left[\left(\frac{c_p - c_v}{c_p}\right)\arctan(q_d\xi) + \frac{c_v}{c_p}(q_d\xi)\right], \text{ and} \tag{46}$$

$$\Omega_0 = \frac{2}{\pi}\left[1 - \exp\left(\frac{-1}{(q_d\xi)^{-1} + \frac{1}{3}\left(\frac{(q_d\xi)\rho_c}{\rho}\right)^2}\right)\right]. \tag{47}$$

The heat capacity at constant volume, $c_v(T,\rho)$, is obtained from the equation of state, and the correlation length ξ is given by

$$\xi = \xi_0\left[\frac{p_c\rho}{\Gamma\rho_c^2}\right]^{\nu/\gamma}\left[\left.\frac{\partial\rho(T,\rho)}{\partial p}\right|_T - \frac{T_R}{T}\left.\frac{\partial\rho(T_R,\rho)}{\partial p}\right|_T\right]^{\nu/\gamma}. \tag{48}$$

The partial derivative $\partial\rho/\partial p|_T$ is evaluated with the equation of state at the system temperature T and a reference temperature, T_R. For the reference temperature, we select a value where the critical enhancement is assumed to be negligible: $T_R = 1.5T_c$. The exponents $\gamma = 1.239$ and $\nu = 0.63$ are universal constants. The critical amplitudes Γ and ξ_0 are system-dependent and are determined by the asymptotic behavior of the equation of state in the critical region. The thermal conductivity at the critical point itself is infinite. We have chosen to use fixed values that we consider reasonable, $\Gamma = 0.0496$ and $\xi_0 = 1.94\cdot10^{-10}$ m. The only parameter left to be determined is the cutoff wavenumber q_d (or alternatively, its inverse q_d^{-1}). If there are sufficient data available in the critical region, we fit thermal conductivity data to determine the system-dependent cutoff parameter q_d^{-1}. Data were unavailable in the critical region so we have estimated the value of q_d^{-1} to be approximately $1.52\cdot10^{-9}$ m; this is the same value we used for dodecane[42].

Figure 26 shows comparisons of the model with experimental thermal conductivity data obtained at NIST, and with values obtained from the graph presented in the Handbook of Aviation Fuel Properties [29] as a function of temperature. The values from the Handbook of Aviation Fuel Properties are approximately 5 to 7 % higher than the model predictions. The deviations with the NIST data are less than 2 %. The NIST data cover pressures up to 30 MPa, while the handbook data are for atmospheric pressure only. Figure 27 shows the deviations in thermal conductivity as a function of pressure. The deviations remain less than 2 % even at 30 MPa. We note however that density data at pressures above atmospheric were unavailable for the development of the equation of state and this could lead to uncertainties in the density at higher pressures; which in turn can lead to larger uncertainties in the transport properties at higher pressures. It is therefore important to obtain reliable measurements of the density at higher pressures to validate the behavior of both the equation of state and the transport properties at pressures above atmospheric.
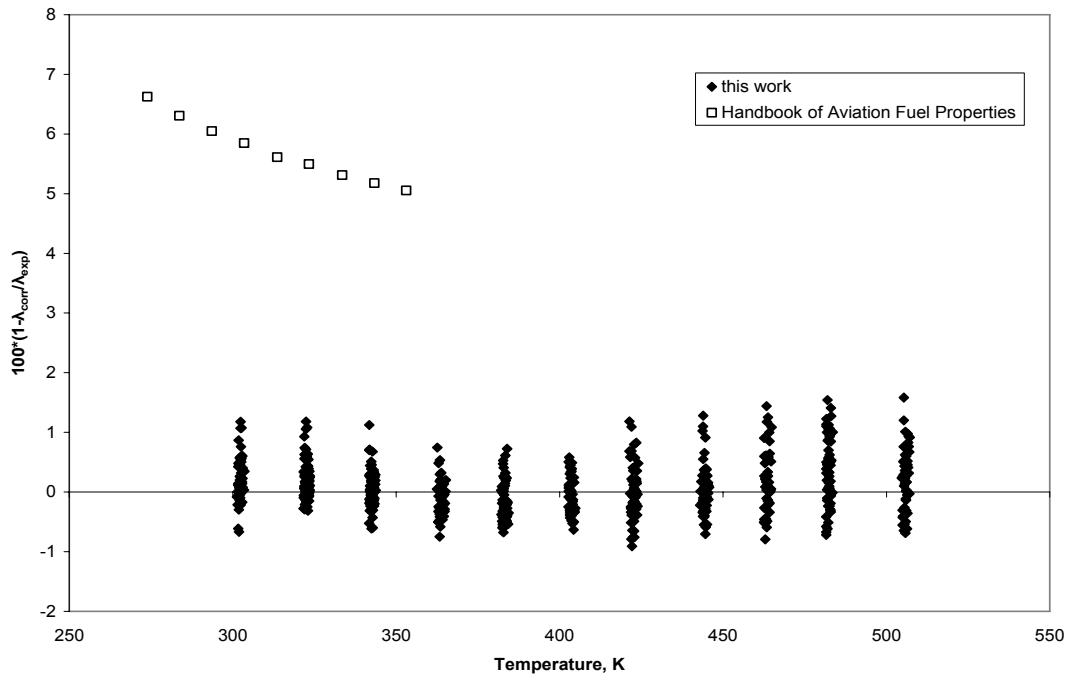
Figure 26. Thermal conductivity deviations as a function of temperature.
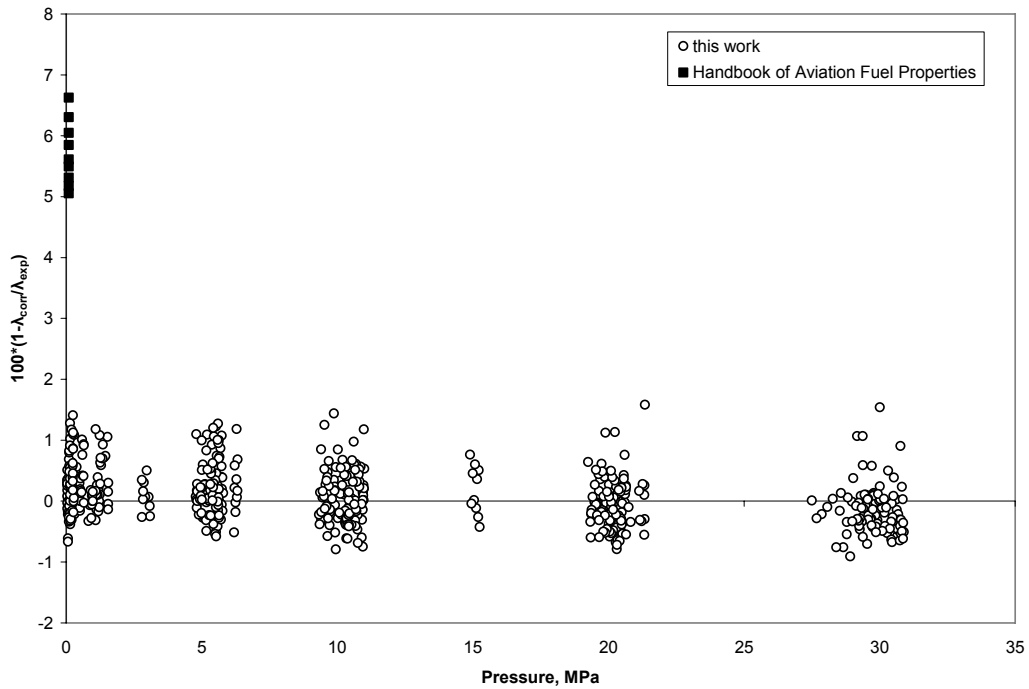
Figure 27. Thermal conductivity deviations as a function of pressure.

References

[1]   Davidson, D. F.; Horning, D. C.; Herbon, J. T.; Hanson, R. K. Shock tube measurements of jp-10 ignition. *Proceedings of the Combustion Institute*, 28: 1687-1692; 2000.

[2]   Cooper, M.; Shepherd, J. E. Experiments studying thermal cracking, catalytic cracking and pre-mixed partial oxidation of JP-10. *AIAA/ASME/SAE/ASEE Joint Propulsion Conference,* July 20-23, Huntsville, AL, Paper 2003-4687: 1-20; 2003.

[3]   Yu, J.; Esser, S. Supercritical phase thermal decomposition of binary mixtures of jet fuel model compounds. *Fuel*, 79: 759-768; 2000.

[4]   Wohlwend, K.; Maurice, L. Q.; Edwards, T.; Striebich, R. C.; Vangsness, M.; Hill, A. S. Thermal stability of energetic hydrocarbon fuels for use in combined cycle engines. *Journal of Propulsion and Power*, 17: 1258-1262; 2001.

[5]   Striebich, R. C.; Lawrence, J. Thermal decomposition of high-energy density materials at high pressure and temperature. *Journal of Analytical and Applied Pyrolysis*, 70: 339-352; 2003.

[6]   Song, C. S.; Eser, S.; Schobert, H. H.; Hatcher, P. G. Pyrolytic degradation studies of a coal-derived and a petroleum-derived aviation jet fuel. *Energy & Fuels*, 7: 234-243 1993.

[7]   Peters, J. E.; Mellor, A. M. Liquid fuel spray ignition predictions for JP-10. *Journal of Energy*, 7: 95-96; 1983.

[8]   Nakra, S.; Green, R. J.; Anderson, S.L. Thermal decomposition of JP-10 studied by micro-flowtube pyrolysis-mass spectrometry. *Proceedings of the Fifteenth ONR Propulsion Meeting*, 234-239; 2002.

[9]   Andersen, W. A.; Bruno, T. J. Rapid screening of fluids for chemical stability in organic rankine cycle applications. *Industrial & Engineering Chemistry Research*, 44: 5560-5566; 2005.

[10]   Andersen, P. C.; Bruno, T. J. Thermal decomposition kinetics of RP-1 rocket propellant. *Industrial & Engineering Chemistry Research*, 44: 1670-1676, 2005.

[11]   House, J. E. *Principles of Chemical Kinetics*; William C. Brown Publishers, Times Mirror Higher Education Group, Inc.: Dubuque, IA; 1997.

[12]   Fodor, G. E.; Naegeli, D.W. Peroxide formation in jet fuels. *Energy & Fuels*, 2: 729-734; 1988.

[13]   Lorant, G. E.; Behar, F.; Vandenbroucke, M.; McKinney, D. E.; Tang, Y. Methane generation from methylated aromatics: Kinetic study and carbon isotope modeling. *Energy & Fuels*, 14: 1143-1155; 2000.

[14]   A modification of: Lemmon, E. W.; McLinden, M. O.; Huber, M. L. REFPROP, Reference fluid thermodynamic and transport properties; Natl. Inst. Stand. Technol. NIST Standard Reference Database 23, Version 7; 2002.

[15]   Perkins, R. A.; Roder, H.M.; Nieto de Castro, C.A. A High-Temperature Transient Hot-Wire Thermal Conductivity Apparatus for Fluids. Natl. Inst. Stand. Technol. Journal of Research 96: 247-269; 1991.

[16]   Nieto de Castro, C. A.; Perkins, R.A.; Roder, H. M. Radiative heat transfer in transient hot-wire measurements of thermal conductivity. *International Journal of Thermophyics.*, 12: 985-997; 1991.

[17]   Bruno, T. J. Improvements in the measurement of distillation curves - part 1: a composition-explicit approach. *Industrial & Engineering Chemistry Research, submitted* 2005.

[18]   OECD Guideline for the testing of chemicals, No. 103, boiling point. Adopted by the council 27 July, *Organisation for Economic Co-operation and Development,* Paris, France; 1995.

[19]   Steele, W. V.; Chirico, R. D.; Knipmeyer, S. E.; Smith, N. K. *High-temperature heat-capacity measurements and critical property determinations using a differential scanning calorimeter--results of measurements on toluene, tetralin, and JP-10 NIPER-395*, National Institute for Petroleum and Energy Research, Bartlesville, OK; 1989.

[20]   Moynihan, C. T.; Shahriari, M.; Mossadegh, R.; Adel-Hadadi, M.; Boulos, E. N. *Melting point and vViscosity behavior of high energy density missile fuels AFWAL-TR-82-2025*, Catholic University of America, Washington, DC; 1982.

[21]   Boyd, R.; Sanwal, S.; Shary-Tahrany, S.; McNally, D. The thermochemistry, thermodynamic functions, and molecular structures of some cyclic hydrocarbons. *Journal of Physical Chemistry* 75: 1264-1271; 1971.

[22]   Moynihan, C. T.; Schnaus, U. E.; Sasabe, H.; Czaplak, D. S. *Physical properties of hydrogenated dimers of norbornadiene and exo-tetrahydrodicyclopentadiene and their mixtures.* Research supported by contract no. N00019-77-C-0065, Naval Air Systems Command, Catholic University of America, Washington, DC; 1977.

[23]   Moynihan, C. T.; Sasabe, H.; Czaplak, D. S.; Schnaus, U. E. Enthalpies of fusion, heat capacities, densities and shear viscosities of hydrogenated dimers of norbornadiene and cyclopentadiene. *Journal of Chemical and Engineering Data,* 23: 107-111; 1978.

[24]   Smith, N. K.; Scott, D. W.; Lee-Bechtold, S.; Osborn, A. G.; Good, W. D. *Thermodynamics of organic compounds AFOSR-TR-79-0197*, Bartlesville Energy Technology Center, Bartlesville, OK; 1978.

[25]   Smith, N. K.; Good, W. D. Enthalpies of combustion of ramjet fuels. *AIAA Journal,* 17: 905-907; 1979.

[26]   Smith, N. K.; Thomas, R. H. P.; Gammon, B. E.; Lee-Bechtold, S.; Callanan, J. E.; Good, W. D. *Thermodynamics of organic compounds AFOSR-TR-89-0513*, Bartlesville Energy Technology Center, Bartlesville, OK; 1980.

[27]   Gammon, B. E.; Smith, N. K. *Thermodynamics of organic compounds, AFOSR-TR-83-0047*, Bartlesville Energy Technology Center, Bartlesville, OK; 1982.

[28]   Chickos, J. S.; Hillesheim, D.; Nichols, G.; Zehe, M. J. The enthalpies of vaporization and sublimation of exo- and endo-tetrahydrodicyclopentadienes at T=298.15 K. *Journal of Chemical Thermodynamics*, 34: 1647-1658; 2002.

[29]   *Handbook of aviation fuel properties,* CRC Report No. 635, third edition, Coordinating Research Council, Inc (CRC), Alpharetta, GA; 2004.

[30]   Lemmon, E. W.; Jacobsen, R. T.; Penoncello, S. G.; Friend, D. G. Thermodynamic properties of air and mixtures of nitrogen, argon, and oxygen from 60 to 2000 K at pressures to 2000 MPa. *Journal of Physical and Chemical Reference Data,* 29: 331-385; 2000.

[31]   Huber, M. L.; Laesecke, A.; Perkins, R. A. Model for the viscosity and thermal conductivity of refrigerants, including a new correlation for the viscosity of R134a. *Industrial and Engineering Chemistry Research*, 42: 3163-3178; 2003.

[32]   Ely, J. F.; Hanley, H. J. M. Prediction of Transport Properties. 1. Viscosity of fluids and mixtures. *Industrial and Engineering Chemistry Fundamentals*, 20: 323-332; 1981.

[33]   Buecker, D.; Wagner, W. Reference equations of state for the thermodynamic properties of fluid phase n-butane and isobutane. *Journal of Physical and Chemical Reference Data*, *submitted*.

[34]   Vogel, E.; Kuchenmeister, C.; Bich, E.; Laesecke, A. Reference correlation of the viscosity of propane. *Journal of Physical and Chemical Reference Data*, 27: 947-970; 1998.

[35]   Marsh, K. N.; Perkins, R. A.; Ramires, M. L. V. Measurement and correlation of the thermal conductivity of propane from 86 K to 600 K at pressures to 70 MPa. *Journal of Chemical and Engineering Data*, 47: 932-940; 2002.

[36]   McLinden, M. O.; Klein, S. A.; Perkins, R. A. An extended corresponding states model for the thermal conductivity of pure refrigerants and refrigerant mixtures. *International Journal of Refrigeration*, 23: 43-63; 2000.

[37]   Neufeld, P. D.; Janzen, A. R.; Aziz, R. A. Empirical equations to calculate 16 of the transport collision integrals $\Omega(l,s)^*$ for the Lennard-Jones (12-6) potential. *Journal of Chemical Physics*, 57: 1100-1102; 1972.

[38]   Chung, T. H.; Ajlan, L.;Lee, L. L.;Starling, K. E. Generalized multiparameter correlation for nonpolar and polar fluid transport properties. *Industrial and Engineering Chemistry Research*, 27: 671-679; 1988.

[39]   Ely, J. F.; Hanley, H. J. M. Prediction of transport properties. 2. Thermal conductivity of pure fluids and mixtures. *Industrial and Engineering Chemisty Fundamentals*, 22: 90-97; 1983.

[40]   Mohr, P. J.; Taylor, B. N. CODATA recommended values of the fundamental physical constants: 1998. *Reviews of Modern Physics*, 77: 1-107; 2005.

[41]   Olchowy, G. A.; Sengers, J. V. A simplified representation for the thermal conductivity of fluids in the critical region. *International Journal of Thermophysics*, 10:, 417-426; 1989.

[42]   Huber, M. L.; Laesecke, A.; Perkins, R.A. Transport properties of n-dodecane. *Energy and Fuels*, 18(4): p. 968-975; 2004.

Appendix 1. Thermal conductivity measurements of liquid JP-10

Point ID	T_0 (K)	T_e (K)	P_e (MPa)	ρ_e (mol·L^{-1})	λ_e (W·m^{-1}K^{-1})
1011	300.209	301.677	0.067	6.8157	0.11105
1012	300.205	301.706	0.067	6.8156	0.11166
1013	300.209	301.960	0.067	6.8141	0.11096
1014	300.207	301.995	0.067	6.8139	0.11177
1015	300.209	302.245	0.067	6.8125	0.11180
1016	300.211	302.373	0.066	6.8117	0.11141
1017	300.209	302.912	0.066	6.8086	0.11140
1018	300.209	303.057	0.066	6.8078	0.11167
1019	300.210	303.441	0.066	6.8056	0.11158
1020	300.213	303.574	0.066	6.8048	0.11191
1021	300.198	301.731	5.669	6.8419	0.11321
1022	300.201	301.816	5.694	6.8415	0.11407
1023	300.196	302.115	5.713	6.8399	0.11289
1024	300.197	302.156	5.732	6.8398	0.11370
1025	300.194	302.451	5.728	6.8381	0.11347
1026	300.194	302.556	5.747	6.8376	0.11324
1027	300.191	302.794	5.759	6.8363	0.11343
1028	300.191	302.725	5.741	6.8366	0.11423
1029	300.187	302.885	5.606	6.8351	0.11311
1030	300.185	302.956	5.506	6.8342	0.11318
1031	300.171	301.796	10.941	6.8656	0.11448
1032	300.166	301.869	10.941	6.8652	0.11446
1033	300.165	302.191	10.966	6.8635	0.11458
1034	300.162	302.190	10.978	6.8636	0.11451
1035	300.162	302.470	10.997	6.8622	0.11487
1036	300.156	302.407	10.983	6.8624	0.11562
1037	300.156	302.529	10.860	6.8612	0.11487
1038	300.156	302.583	10.761	6.8605	0.11478
1039	300.151	302.834	10.690	6.8588	0.11486
1040	300.153	302.949	10.631	6.8579	0.11482
1041	300.123	301.660	20.565	6.9085	0.11701
1042	300.118	301.731	20.586	6.9083	0.11664
1043	300.119	301.981	20.601	6.9070	0.11647
1044	300.113	302.057	20.617	6.9067	0.11662
1045	300.115	302.342	20.637	6.9053	0.11668
1046	300.113	302.400	20.644	6.9050	0.11676
1047	300.109	302.615	20.652	6.9039	0.11672
1048	300.106	302.523	20.594	6.9041	0.11733
1049	300.107	302.745	20.472	6.9024	0.11667
1050	300.105	302.836	20.388	6.9016	0.11657
1051	300.095	301.546	29.851	6.9479	0.11854
1052	300.097	301.649	29.777	6.9471	0.11867
1053	300.092	301.875	29.699	6.9456	0.11813
1054	300.091	301.930	29.627	6.9450	0.11848
1055	300.091	302.214	29.557	6.9433	0.11837
1056	300.086	302.277	29.485	6.9427	0.11829
1057	300.090	302.386	29.383	6.9417	0.11907

Point ID	T_0	T_e	P_e	ρ_e	λ_e
	(K)	(K)	(MPa)	(mol·L^{-1})	(W·m^{-1}K^{-1})
1058	300.085	302.376	29.172	6.9409	0.11961
1059	300.087	302.619	28.981	6.9389	0.11826
1060	300.085	302.680	28.824	6.9379	0.11830
1061	300.029	301.290	0.299	6.8191	0.11174
1062	300.031	301.458	0.316	6.8182	0.11157
1063	300.024	301.764	0.335	6.8165	0.11232
1064	300.029	301.920	0.349	6.8157	0.11191
1065	300.023	302.139	0.359	6.8145	0.11226
1066	300.027	302.273	0.369	6.8138	0.11225
1067	300.017	302.590	0.378	6.8120	0.11207
1068	300.022	302.662	0.386	6.8116	0.11233
1069	300.024	303.033	0.393	6.8095	0.11211
1070	300.024	303.112	0.399	6.8091	0.11206
1071	320.274	321.984	0.174	6.6994	0.10937
1072	320.269	322.013	0.182	6.6993	0.11017
1073	320.268	322.346	0.188	6.6974	0.10956
1074	320.266	322.379	0.194	6.6972	0.10991
1075	320.259	322.702	0.199	6.6954	0.10986
1076	320.258	322.773	0.203	6.6950	0.10959
1077	320.255	323.057	0.207	6.6934	0.10985
1078	320.252	322.920	0.207	6.6942	0.11008
1079	320.245	323.141	0.205	6.6929	0.10996
1080	320.242	323.214	0.203	6.6924	0.10948
1081	320.240	322.193	1.549	6.7055	0.11000
1082	320.243	322.212	1.545	6.7054	0.10978
1083	320.247	322.497	1.543	6.7037	0.10965
1084	320.247	322.247	1.555	6.7052	0.11016
1085	320.251	322.454	1.525	6.7039	0.11097
1086	320.249	322.410	1.393	6.7034	0.11056
1087	320.247	322.664	1.291	6.7014	0.11036
1088	320.253	322.778	1.231	6.7004	0.11088
1089	320.254	323.077	1.194	6.6985	0.10987
1090	320.260	323.191	1.163	6.6977	0.11005
1091	320.253	322.018	1.445	6.7059	0.11065
1092	320.251	321.881	1.355	6.7063	0.11085
1093	320.250	322.079	1.254	6.7046	0.11047
1094	320.248	322.122	1.190	6.7040	0.10994
1095	320.248	322.404	1.139	6.7021	0.10999
1096	320.253	322.440	1.092	6.7017	0.11099
1097	320.242	322.746	1.053	6.6997	0.10960
1098	320.245	322.995	1.091	6.6985	0.10928
1099	320.247	323.386	1.183	6.6967	0.10962
1100	320.246	323.620	1.241	6.6957	0.10971
1101	320.257	321.740	5.037	6.7263	0.11052
1102	320.259	321.908	5.115	6.7258	0.11053
1103	320.257	322.266	5.177	6.7241	0.11078
1104	320.253	322.312	5.209	6.7240	0.11099
1105	320.254	322.641	5.232	6.7222	0.11102
1106	320.253	322.735	5.242	6.7218	0.11090
1107	320.255	322.990	5.250	6.7204	0.11098

Point ID	T_0	T_e	P_e	ρ_e	λ_e
	(K)	(K)	(MPa)	(mol·L^{-1})	(W·m^{-1}K^{-1})
1108	320.253	323.169	5.259	6.7194	0.11086
1109	320.255	323.454	5.266	6.7178	0.11071
1110	320.258	323.613	5.279	6.7170	0.11098
1111	320.248	321.707	10.112	6.7523	0.11254
1112	320.240	321.695	10.019	6.7519	0.11182
1113	320.243	321.992	9.945	6.7499	0.11271
1114	320.242	322.006	9.876	6.7494	0.11245
1115	320.239	322.289	9.822	6.7476	0.11200
1116	320.236	322.473	9.812	6.7465	0.11189
1117	320.232	322.805	9.855	6.7449	0.11183
1118	320.228	322.982	9.904	6.7442	0.11224
1119	320.227	323.316	9.914	6.7424	0.11187
1120	320.223	323.399	9.920	6.7420	0.11213
1121	320.246	321.813	19.957	6.7994	0.11453
1122	320.250	321.922	19.910	6.7986	0.11472
1123	320.246	322.093	19.848	6.7974	0.11434
1124	320.248	322.213	19.808	6.7966	0.11442
1125	320.254	322.483	19.747	6.7949	0.11442
1126	320.253	322.520	19.701	6.7945	0.11491
1127	320.253	322.859	19.652	6.7924	0.11465
1128	320.256	322.908	19.590	6.7919	0.11441
1129	320.260	323.240	19.548	6.7899	0.11436
1130	320.255	323.337	19.484	6.7891	0.11435
1131	320.260	321.773	20.167	6.8006	0.11462
1132	320.261	321.885	20.134	6.7999	0.11507
1133	320.260	322.106	20.077	6.7984	0.11453
1134	320.263	322.192	20.042	6.7978	0.11447
1135	320.265	322.489	19.991	6.7960	0.11440
1136	320.263	322.513	19.951	6.7957	0.11463
1137	320.268	322.883	19.909	6.7935	0.11449
1138	320.264	322.915	19.859	6.7931	0.11496
1139	320.267	323.262	19.822	6.7911	0.11455
1140	320.267	323.358	19.769	6.7904	0.11427
1141	320.282	321.775	29.985	6.8455	0.11693
1142	320.281	321.899	29.883	6.8444	0.11708
1143	320.284	322.099	29.769	6.8429	0.11663
1144	320.286	322.200	29.681	6.8420	0.11696
1145	320.282	322.455	29.578	6.8403	0.11667
1146	320.281	322.512	29.494	6.8396	0.11699
1147	320.283	322.846	29.401	6.8375	0.11653
1148	320.286	322.882	29.311	6.8369	0.11689
1149	320.284	323.239	29.228	6.8347	0.11672
1150	320.284	323.304	29.132	6.8339	0.11663
1151	320.275	321.891	0.165	6.6999	0.10956
1152	320.276	321.950	0.168	6.6995	0.10977
1153	320.274	322.235	0.170	6.6979	0.10939
1154	320.278	322.296	0.172	6.6976	0.11007
1155	320.279	322.630	0.174	6.6957	0.10967
1156	320.277	322.651	0.175	6.6955	0.11007
1157	320.282	323.054	0.177	6.6932	0.10967

Point ID	T_0 (K)	T_e (K)	P_e (MPa)	ρ_e (mol·L^{-1})	λ_e (W·m^{-1}K^{-1})
1158	320.283	323.090	0.178	6.6930	0.10962
1159	320.282	323.472	0.180	6.6908	0.10969
1160	320.279	323.541	0.181	6.6904	0.10957
1161	320.292	322.013	5.127	6.7252	0.11093
1162	320.294	322.009	5.120	6.7252	0.11113
1163	320.296	322.326	5.118	6.7234	0.11107
1164	320.297	322.346	5.103	6.7232	0.11105
1165	320.299	322.661	5.104	6.7215	0.11100
1166	320.302	322.723	5.086	6.7210	0.11077
1167	320.299	323.045	5.088	6.7192	0.11085
1168	320.302	323.145	5.072	6.7186	0.11072
1169	320.299	323.419	5.071	6.7170	0.11087
1170	320.300	323.569	5.052	6.7161	0.11067
1171	340.586	342.092	5.500	6.6137	0.10872
1172	340.584	342.237	5.514	6.6130	0.10897
1173	340.584	342.455	5.526	6.6118	0.10829
1174	340.580	342.540	5.538	6.6114	0.10914
1175	340.584	342.843	5.544	6.6097	0.10837
1176	340.582	342.885	5.553	6.6095	0.10878
1177	340.586	343.218	5.555	6.6076	0.10862
1178	340.589	343.285	5.555	6.6073	0.10872
1179	340.583	343.611	5.563	6.6054	0.10873
1180	340.588	343.735	5.557	6.6047	0.10854
1181	340.560	341.797	1.344	6.5913	0.10824
1182	340.556	341.840	1.274	6.5906	0.10823
1183	340.551	342.040	1.218	6.5891	0.10742
1184	340.543	342.067	1.164	6.5887	0.10751
1185	340.540	342.343	1.120	6.5868	0.10747
1186	340.530	342.410	1.086	6.5862	0.10751
1187	340.524	342.815	1.121	6.5841	0.10714
1188	340.522	343.019	1.186	6.5833	0.10711
1189	340.517	343.288	1.223	6.5819	0.10716
1190	340.510	343.468	1.260	6.5811	0.10757
1191	340.573	341.986	10.530	6.6425	0.11016
1192	340.568	342.067	10.530	6.6421	0.11018
1193	340.574	342.260	10.525	6.6410	0.11006
1194	340.574	342.355	10.519	6.6404	0.11053
1195	340.574	342.444	10.449	6.6395	0.10998
1196	340.571	342.441	10.335	6.6389	0.10936
1197	340.579	342.730	10.257	6.6369	0.11010
1198	340.579	342.794	10.193	6.6362	0.11071
1199	340.576	343.102	10.148	6.6342	0.10967
1200	340.575	343.206	10.113	6.6335	0.11002
1201	340.584	341.824	20.016	6.6940	0.11309
1202	340.582	341.783	19.885	6.6935	0.11403
1203	340.582	341.992	19.747	6.6917	0.11249
1204	340.589	342.042	19.641	6.6909	0.11316
1205	340.587	342.284	19.538	6.6891	0.11255
1206	340.591	342.345	19.446	6.6883	0.11237
1207	340.598	342.633	19.374	6.6864	0.11229

Point ID	T_0	T_e	P_e	ρ_e	λ_e
	(K)	(K)	(MPa)	(mol·L^{-1})	(W·m^{-1}K^{-1})
1208	340.594	342.838	19.347	6.6851	0.11183
1209	340.596	343.189	19.376	6.6834	0.11231
1210	340.596	343.362	19.366	6.6824	0.11223
1211	340.604	341.833	29.990	6.7438	0.11526
1212	340.599	341.928	29.916	6.7430	0.11502
1213	340.597	342.110	29.846	6.7417	0.11507
1214	340.595	342.242	29.775	6.7407	0.11544
1215	340.595	342.435	29.694	6.7393	0.11494
1216	340.596	342.556	29.632	6.7384	0.11518
1217	340.594	342.771	29.541	6.7369	0.11516
1218	340.595	342.939	29.482	6.7358	0.11509
1219	340.596	343.190	29.400	6.7341	0.11499
1220	340.595	343.332	29.339	6.7331	0.11498
1221	340.613	341.737	30.277	6.7457	0.11488
1222	340.609	341.841	30.176	6.7447	0.11523
1223	340.616	342.060	30.086	6.7432	0.11529
1224	340.611	342.184	30.009	6.7421	0.11566
1225	340.606	342.393	29.922	6.7407	0.11533
1226	340.609	342.509	29.851	6.7397	0.11529
1227	340.611	342.766	29.748	6.7379	0.11477
1228	340.614	342.876	29.671	6.7370	0.11488
1229	340.616	343.203	29.581	6.7349	0.11491
1230	340.608	343.262	29.502	6.7342	0.11524
1231	340.595	341.936	0.498	6.5855	0.10753
1232	340.595	342.092	0.511	6.5846	0.10703
1233	340.595	342.274	0.503	6.5835	0.10705
1234	340.597	342.398	0.517	6.5829	0.10737
1235	340.600	342.673	0.512	6.5813	0.10715
1236	340.598	342.776	0.523	6.5807	0.10730
1237	340.604	343.095	0.523	6.5789	0.10708
1238	340.602	343.118	0.527	6.5788	0.10748
1239	340.602	343.505	0.530	6.5765	0.10703
1240	340.604	343.558	0.525	6.5762	0.10716
1241	340.615	341.991	0.046	6.5825	0.10694
1242	340.618	342.057	0.047	6.5821	0.10737
1243	340.616	342.338	0.047	6.5804	0.10712
1244	340.621	342.381	0.047	6.5802	0.10757
1245	340.615	342.700	0.048	6.5783	0.10717
1246	340.616	342.760	0.048	6.5780	0.10694
1247	340.616	343.057	0.048	6.5762	0.10732
1248	340.616	343.154	0.048	6.5757	0.10729
1249	340.620	343.458	0.048	6.5739	0.10716
1250	340.622	343.623	0.048	6.5729	0.10718
1251	361.305	362.909	0.820	6.4646	0.10439
1252	361.298	363.027	0.877	6.4643	0.10466
1253	361.293	363.299	0.908	6.4629	0.10490
1254	361.284	363.383	0.929	6.4626	0.10442
1255	361.278	363.640	0.942	6.4611	0.10462
1256	361.265	363.736	0.954	6.4606	0.10476
1257	361.250	364.006	0.963	6.4591	0.10464

Point ID	T_0	T_e	P_e	ρ_e	λ_e
	(K)	(K)	(MPa)	(mol·L^{-1})	(W·m^{-1}K^{-1})
1258	361.244	364.111	0.972	6.4586	0.10474
1259	361.229	364.413	0.980	6.4568	0.10459
1260	361.214	364.508	0.985	6.4563	0.10474
1261	361.152	362.500	5.605	6.4981	0.10639
1262	361.168	362.579	5.557	6.4973	0.10711
1263	361.183	362.882	5.522	6.4954	0.10574
1264	361.207	362.986	5.518	6.4948	0.10599
1265	361.226	363.412	5.583	6.4927	0.10578
1266	361.240	363.624	5.655	6.4920	0.10621
1267	361.260	363.960	5.705	6.4904	0.10588
1268	361.277	364.106	5.740	6.4898	0.10613
1269	361.291	364.429	5.768	6.4881	0.10599
1270	361.307	364.571	5.792	6.4874	0.10629
1271	361.293	363.324	10.944	6.5267	0.10713
1272	361.288	363.367	10.959	6.5265	0.10803
1273	361.288	363.645	10.973	6.5251	0.10792
1274	361.279	363.663	10.981	6.5250	0.10813
1275	361.280	363.763	10.912	6.5241	0.10754
1276	361.276	363.796	10.820	6.5233	0.10819
1277	361.281	364.057	10.755	6.5215	0.10755
1278	361.281	364.146	10.703	6.5207	0.10774
1279	361.283	364.473	10.661	6.5186	0.10772
1280	361.284	364.677	10.658	6.5174	0.10735
1281	361.348	362.951	20.129	6.5828	0.11019
1282	361.351	363.015	20.049	6.5820	0.11125
1283	361.355	363.330	20.011	6.5801	0.11026
1284	361.348	363.499	20.042	6.5794	0.11002
1285	361.353	363.908	20.091	6.5775	0.11017
1286	361.352	364.024	20.106	6.5770	0.11053
1287	361.354	364.354	20.102	6.5752	0.11038
1288	361.354	364.466	20.097	6.5746	0.11034
1289	361.346	364.779	20.090	6.5729	0.11019
1290	361.350	364.937	20.084	6.5721	0.11032
1291	361.450	363.390	30.070	6.6352	0.11302
1292	361.452	363.452	29.987	6.6345	0.11354
1293	361.449	363.700	29.917	6.6328	0.11306
1294	361.454	363.548	29.768	6.6328	0.11356
1295	361.456	363.777	29.582	6.6307	0.11304
1296	361.460	363.817	29.442	6.6297	0.11346
1297	361.459	364.088	29.346	6.6278	0.11291
1298	361.458	364.196	29.267	6.6268	0.11274
1299	361.458	364.587	29.247	6.6248	0.11276
1300	361.459	364.818	29.274	6.6237	0.11288
1301	361.436	363.380	0.157	6.4574	0.10501
1302	361.439	363.387	0.157	6.4574	0.10476
1303	361.438	363.583	0.158	6.4562	0.10428
1304	361.441	363.678	0.159	6.4557	0.10462
1305	361.441	363.915	0.160	6.4543	0.10435
1306	361.440	364.090	0.163	6.4533	0.10438
1307	361.443	364.543	0.170	6.4506	0.10425

Point ID	T_0	T_e	P_e	ρ_e	λ_e
	(K)	(K)	(MPa)	(mol·L^{-1})	(W·m^{-1}K^{-1})
1308	361.447	364.752	0.176	6.4494	0.10424
1309	361.446	365.092	0.181	6.4474	0.10425
1310	361.447	365.256	0.184	6.4465	0.10443
1311	380.665	382.692	9.643	6.4099	0.10472
1312	380.657	382.696	9.650	6.4099	0.10582
1313	380.639	382.697	9.610	6.4096	0.10497
1314	380.622	382.743	9.529	6.4088	0.10583
1315	380.615	382.932	9.460	6.4073	0.10529
1316	380.599	383.028	9.408	6.4064	0.10488
1317	380.590	383.298	9.365	6.4046	0.10530
1318	380.588	383.399	9.328	6.4037	0.10490
1319	380.573	383.821	9.349	6.4015	0.10469
1320	380.572	384.046	9.411	6.4007	0.10489
1321	380.522	382.414	0.196	6.3442	0.10185
1322	380.513	382.526	0.199	6.3436	0.10202
1323	380.501	382.805	0.201	6.3419	0.10226
1324	380.490	382.894	0.203	6.3414	0.10240
1325	380.480	383.183	0.205	6.3396	0.10163
1326	380.473	383.293	0.206	6.3390	0.10204
1327	380.468	383.421	0.206	6.3382	0.10217
1328	380.462	383.393	0.201	6.3384	0.10254
1329	380.465	383.715	0.196	6.3364	0.10173
1330	380.459	383.810	0.194	6.3358	0.10210
1331	380.508	382.124	5.413	6.3838	0.10396
1332	380.503	382.261	5.436	6.3832	0.10353
1333	380.487	382.624	5.491	6.3814	0.10334
1334	380.482	382.733	5.528	6.3811	0.10400
1335	380.464	383.014	5.560	6.3797	0.10361
1336	380.457	383.159	5.585	6.3790	0.10413
1337	380.455	383.452	5.604	6.3774	0.10369
1338	380.449	383.582	5.623	6.3768	0.10403
1339	380.448	383.924	5.642	6.3750	0.10351
1340	380.444	383.932	5.653	6.3750	0.10455
1341	380.602	382.512	10.907	6.4195	0.10513
1342	380.613	382.583	10.922	6.4192	0.10562
1343	380.623	382.875	10.936	6.4176	0.10558
1344	380.632	382.912	10.939	6.4174	0.10575
1345	380.640	383.045	10.898	6.4164	0.10565
1346	380.644	383.083	10.813	6.4156	0.10592
1347	380.647	383.324	10.746	6.4138	0.10513
1348	380.652	383.412	10.697	6.4130	0.10593
1349	380.651	383.760	10.673	6.4109	0.10511
1350	380.659	384.014	10.705	6.4097	0.10535
1351	380.709	382.381	20.288	6.4808	0.10893
1352	380.709	382.425	20.250	6.4803	0.10829
1353	380.711	382.806	20.267	6.4784	0.10805
1354	380.722	383.014	20.334	6.4777	0.10848
1355	380.726	383.338	20.390	6.4764	0.10838
1356	380.734	383.491	20.432	6.4758	0.10827
1357	380.736	383.791	20.464	6.4744	0.10822

Point ID	T_0 (K)	T_e (K)	P_e (MPa)	ρ_e (mol·L^{-1})	λ_e (W·m^{-1}K^{-1})
1358	380.743	383.935	20.489	6.4738	0.10854
1359	380.747	384.280	20.512	6.4721	0.10813
1360	380.746	384.409	20.529	6.4715	0.10832
1361	380.848	382.552	30.559	6.5413	0.11151
1362	380.855	382.660	30.593	6.5409	0.11162
1363	380.858	382.923	30.617	6.5397	0.11148
1364	380.860	383.031	30.636	6.5393	0.11180
1365	380.865	383.323	30.652	6.5379	0.11130
1366	380.862	383.401	30.666	6.5376	0.11160
1367	380.864	383.710	30.679	6.5361	0.11138
1368	380.867	383.788	30.687	6.5358	0.11167
1369	380.873	383.889	30.650	6.5351	0.11143
1370	380.873	383.929	30.561	6.5343	0.11143
1371	401.017	402.715	3.090	6.2449	0.10029
1372	401.014	402.816	3.090	6.2443	0.10045
1373	401.000	402.833	3.041	6.2438	0.10058
1374	400.991	402.821	2.970	6.2433	0.10100
1375	400.976	403.020	2.916	6.2417	0.10051
1376	400.960	403.102	2.863	6.2408	0.10072
1377	400.948	403.362	2.832	6.2389	0.10039
1378	400.928	403.670	2.794	6.2368	0.10066
1379	400.908	404.297	2.797	6.2330	0.09997
1380	400.888	404.504	2.844	6.2322	0.10039
1381	400.820	402.798	0.179	6.2204	0.09941
1382	400.836	402.846	0.177	6.2201	0.09950
1383	400.848	402.951	0.169	6.2194	0.09950
1384	400.860	402.957	0.158	6.2192	0.09995
1385	400.873	403.261	0.154	6.2173	0.09895
1386	400.889	403.341	0.151	6.2168	0.09976
1387	400.900	403.638	0.151	6.2150	0.09929
1388	400.916	403.776	0.150	6.2141	0.09975
1389	400.929	404.087	0.150	6.2122	0.09909
1390	400.938	404.367	0.156	6.2105	0.09943
1391	401.352	403.247	10.524	6.2998	0.10286
1392	401.356	403.120	10.470	6.3002	0.10369
1393	401.353	403.390	10.422	6.2983	0.10296
1394	401.357	403.440	10.382	6.2977	0.10306
1395	401.360	403.688	10.345	6.2960	0.10275
1396	401.363	403.773	10.312	6.2953	0.10283
1397	401.363	404.046	10.292	6.2936	0.10293
1398	401.370	404.197	10.287	6.2927	0.10271
1399	401.370	404.581	10.308	6.2906	0.10268
1400	401.370	404.828	10.351	6.2896	0.10274
1401	401.377	403.240	20.307	6.3700	0.10625
1402	401.378	403.329	20.314	6.3695	0.10682
1403	401.372	403.399	20.285	6.3690	0.10694
1404	401.376	403.430	20.230	6.3684	0.10702
1405	401.376	403.643	20.177	6.3669	0.10611
1406	401.380	403.704	20.139	6.3663	0.10703
1407	401.378	403.991	20.101	6.3645	0.10600

Point ID	T_0	T_e	P_e	ρ_e	λ_e
	(K)	(K)	(MPa)	(mol·L^{-1})	(W·m^{-1}K^{-1})
1408	401.381	404.062	20.072	6.3640	0.10633
1409	401.380	404.347	20.052	6.3623	0.10598
1410	401.380	404.543	20.055	6.3613	0.10615
1411	401.379	403.213	30.722	6.4383	0.10983
1412	401.378	403.232	30.726	6.4382	0.10978
1413	401.374	403.266	30.677	6.4377	0.10979
1414	401.377	403.314	30.615	6.4371	0.11014
1415	401.382	403.525	30.561	6.4357	0.10964
1416	401.383	403.630	30.528	6.4349	0.11049
1417	401.386	403.863	30.483	6.4335	0.10973
1418	401.387	403.994	30.450	6.4326	0.10996
1419	401.385	404.272	30.433	6.4311	0.10928
1420	401.387	404.428	30.431	6.4303	0.10958
1421	420.018	421.347	6.327	6.1610	0.10022
1422	420.016	421.349	6.284	6.1606	0.10071
1423	420.011	421.585	6.248	6.1589	0.09945
1424	419.988	421.626	6.216	6.1583	0.10004
1425	419.970	421.878	6.194	6.1566	0.09891
1426	419.949	422.054	6.213	6.1558	0.09962
1427	419.931	422.387	6.251	6.1541	0.09920
1428	419.902	422.523	6.280	6.1536	0.09973
1429	419.880	422.833	6.300	6.1519	0.09941
1430	419.852	422.987	6.314	6.1511	0.09950
1431	419.799	421.886	0.106	6.1013	0.09656
1432	419.803	422.032	0.109	6.1005	0.09754
1433	419.821	422.336	0.112	6.0986	0.09676
1434	419.834	422.443	0.114	6.0979	0.09721
1435	419.841	422.799	0.116	6.0957	0.09679
1436	419.864	422.807	0.117	6.0957	0.09755
1437	419.877	422.950	0.116	6.0948	0.09660
1438	419.888	423.047	0.115	6.0941	0.09730
1439	419.900	423.317	0.114	6.0924	0.09663
1440	419.910	423.464	0.114	6.0915	0.09749
1441	419.966	421.912	5.235	6.1480	0.09875
1442	419.975	422.005	5.196	6.1471	0.10009
1443	419.969	422.267	5.159	6.1452	0.09864
1444	419.972	422.389	5.142	6.1443	0.09911
1445	419.979	422.786	5.171	6.1422	0.09841
1446	419.977	423.033	5.230	6.1413	0.09893
1447	419.983	423.404	5.276	6.1394	0.09863
1448	419.986	423.537	5.308	6.1389	0.09903
1449	419.983	423.885	5.336	6.1371	0.09859
1450	419.988	424.051	5.355	6.1363	0.09929
1451	420.057	422.071	10.316	6.1906	0.10064
1452	420.054	422.185	10.351	6.1902	0.10074
1453	420.055	422.463	10.374	6.1888	0.10062
1454	420.057	422.598	10.391	6.1882	0.10112
1455	420.057	422.881	10.406	6.1867	0.10074
1456	420.060	423.035	10.422	6.1859	0.10098
1457	420.059	423.336	10.435	6.1843	0.10054

Point ID	T_0 (K)	T_e (K)	P_e (MPa)	ρ_e (mol·L^{-1})	λ_e (W·m^{-1}K^{-1})
1458	420.061	423.455	10.450	6.1838	0.10072
1459	420.065	423.586	10.436	6.1829	0.10105
1460	420.070	423.644	10.362	6.1819	0.10123
1461	420.140	421.820	20.331	6.2708	0.10456
1462	420.138	421.932	20.310	6.2700	0.10398
1463	420.143	422.290	20.334	6.2683	0.10410
1464	420.144	422.450	20.379	6.2678	0.10452
1465	420.144	422.834	20.418	6.2660	0.10407
1466	420.144	422.940	20.448	6.2656	0.10491
1467	420.147	423.262	20.465	6.2640	0.10442
1468	420.150	423.429	20.482	6.2633	0.10494
1469	420.143	423.736	20.492	6.2617	0.10428
1470	420.145	423.851	20.503	6.2612	0.10464
1471	420.190	422.138	28.922	6.3307	0.10685
1472	420.190	422.235	28.792	6.3293	0.10740
1473	420.194	422.521	28.662	6.3269	0.10688
1474	420.194	422.640	28.533	6.3254	0.10747
1475	420.193	422.885	28.401	6.3233	0.10676
1476	420.189	422.949	28.268	6.3220	0.10756
1477	420.192	423.042	28.073	6.3202	0.10734
1478	420.196	423.156	27.867	6.3182	0.10713
1479	420.199	423.379	27.680	6.3157	0.10697
1480	420.203	423.503	27.502	6.3138	0.10721
2001	441.923	443.655	0.151	5.9631	0.09391
2002	441.896	443.686	0.151	5.9629	0.09434
2003	441.867	443.911	0.151	5.9615	0.09375
2004	441.838	443.792	0.150	5.9622	0.09504
2005	441.806	443.930	0.148	5.9613	0.09457
2006	441.778	443.964	0.147	5.9611	0.09526
2007	441.748	444.214	0.146	5.9594	0.09436
2008	441.716	444.245	0.145	5.9592	0.09401
2009	441.691	444.507	0.144	5.9575	0.09407
2010	441.665	444.637	0.144	5.9567	0.09482
2011	441.702	443.014	4.889	6.0166	0.09610
2012	441.722	443.087	4.858	6.0158	0.09630
2013	441.749	443.355	4.822	6.0138	0.09641
2014	441.768	443.861	4.797	6.0105	0.09724
2015	441.779	444.192	4.788	6.0083	0.09620
2016	441.802	444.409	4.805	6.0072	0.09613
2017	441.807	444.737	4.820	6.0053	0.09597
2018	441.816	444.915	4.831	6.0043	0.09633
2019	441.822	445.259	4.837	6.0022	0.09602
2020	441.828	445.373	4.837	6.0015	0.09616
2021	441.877	443.827	9.742	6.0589	0.09814
2022	441.877	443.955	9.732	6.0580	0.09816
2023	441.883	444.222	9.713	6.0563	0.09787
2024	441.889	444.345	9.688	6.0553	0.09888
2025	441.889	444.635	9.661	6.0534	0.09791
2026	441.895	444.772	9.632	6.0523	0.09855
2027	441.895	445.065	9.603	6.0503	0.09803

Point ID	T_0	T_e	P_e	ρ_e	λ_e
	(K)	(K)	(MPa)	(mol·L^{-1})	(W·m^{-1}K^{-1})
2028	441.898	445.231	9.572	6.0490	0.09835
2029	441.897	445.547	9.543	6.0469	0.09791
2030	441.901	445.700	9.510	6.0456	0.09808
2031	441.969	443.852	20.822	6.1562	0.10243
2032	441.969	443.965	20.742	6.1549	0.10264
2033	441.975	444.232	20.654	6.1527	0.10212
2034	441.974	444.341	20.565	6.1514	0.10301
2035	441.967	444.617	20.472	6.1491	0.10224
2036	441.963	444.713	20.379	6.1479	0.10271
2037	441.965	445.001	20.286	6.1455	0.10223
2038	441.963	445.126	20.194	6.1441	0.10247
2039	441.960	445.449	20.105	6.1416	0.10232
2040	441.960	445.599	20.016	6.1400	0.10239
2041	442.013	443.916	30.198	6.2293	0.10585
2042	442.012	443.978	30.027	6.2277	0.10624
2043	442.016	444.249	29.866	6.2251	0.10569
2044	442.016	444.354	29.705	6.2234	0.10564
2045	442.017	444.629	29.547	6.2208	0.10524
2046	442.026	444.745	29.386	6.2190	0.10529
2047	442.031	444.972	29.220	6.2166	0.10549
2048	442.038	445.019	29.028	6.2149	0.10616
2049	442.048	445.166	28.793	6.2123	0.10509
2050	442.057	445.341	28.576	6.2098	0.10570
2051	460.687	462.668	0.106	5.8375	0.09146
2052	460.693	462.888	0.121	5.8363	0.09213
2053	460.693	463.282	0.164	5.8342	0.09139
2054	460.692	463.462	0.200	5.8334	0.09274
2055	460.701	463.754	0.229	5.8318	0.09149
2056	460.692	463.899	0.247	5.8311	0.09216
2057	460.692	464.254	0.264	5.8289	0.09142
2058	460.697	464.399	0.277	5.8281	0.09157
2059	460.692	464.715	0.289	5.8261	0.09159
2060	460.696	464.889	0.300	5.8251	0.09253
2061	460.722	462.640	5.095	5.8966	0.09431
2062	460.729	462.700	5.042	5.8956	0.09459
2063	460.730	462.962	4.993	5.8934	0.09418
2064	460.733	463.054	4.955	5.8924	0.09417
2065	460.733	463.383	4.939	5.8902	0.09394
2066	460.735	463.615	4.966	5.8890	0.09398
2067	460.735	464.038	4.988	5.8866	0.09368
2068	460.734	464.193	5.001	5.8857	0.09480
2069	460.732	464.551	5.008	5.8836	0.09384
2070	460.734	464.719	5.009	5.8825	0.09428
2071	460.736	462.918	9.945	5.9476	0.09550
2072	460.727	463.036	9.923	5.9466	0.09574
2073	460.726	463.293	9.899	5.9448	0.09636
2074	460.726	463.360	9.875	5.9442	0.09758
2075	460.724	463.393	9.809	5.9433	0.09618
2076	460.731	463.419	9.696	5.9419	0.09633
2077	460.731	463.721	9.605	5.9392	0.09634

Point ID	T_0	T_e	P_e	ρ_e	λ_e
	(K)	(K)	(MPa)	$(mol·L^{-1})$	$(W·m^{-1}K^{-1})$
2078	460.736	463.783	9.529	5.9380	0.09719
2079	460.737	464.065	9.461	5.9356	0.09607
2080	460.744	464.236	9.407	5.9340	0.09669
2081	460.740	462.703	19.945	6.0462	0.10010
2082	460.739	462.827	19.884	6.0449	0.10001
2083	460.738	463.069	19.814	6.0430	0.09998
2084	460.737	463.141	19.741	6.0419	0.10106
2085	460.737	463.416	19.663	6.0397	0.09979
2086	460.735	463.545	19.584	6.0383	0.10010
2087	460.732	463.803	19.499	6.0361	0.10054
2088	460.724	463.928	19.418	6.0346	0.10030
2089	460.721	464.224	19.333	6.0322	0.09982
2090	460.714	464.297	19.250	6.0310	0.10077
2091	460.671	462.559	30.896	6.1404	0.10436
2092	460.671	462.625	30.769	6.1390	0.10580
2093	460.662	462.897	30.639	6.1366	0.10430
2094	460.659	462.958	30.509	6.1353	0.10480
2095	460.658	463.211	30.379	6.1329	0.10417
2096	460.655	463.317	30.244	6.1313	0.10447
2097	460.652	463.556	30.102	6.1289	0.10399
2098	460.655	463.595	29.939	6.1274	0.10456
2099	460.652	463.782	29.751	6.1249	0.10421
2100	460.652	463.920	29.580	6.1228	0.10431
2161	479.267	481.560	0.246	5.7107	0.08982
2162	479.266	481.665	0.251	5.7101	0.09046
2163	479.264	481.934	0.253	5.7082	0.08984
2164	479.262	482.045	0.256	5.7075	0.09020
2165	479.259	482.327	0.257	5.7055	0.09016
2166	479.261	482.293	0.256	5.7058	0.09041
2167	479.261	482.518	0.247	5.7041	0.08965
2168	479.260	482.657	0.243	5.7031	0.08990
2169	479.260	482.924	0.247	5.7013	0.08947
2170	479.266	483.041	0.248	5.7005	0.09057
2171	479.280	481.568	5.531	5.7812	0.09164
2172	479.289	481.657	5.527	5.7806	0.09330
2173	479.287	481.936	5.522	5.7787	0.09203
2175	479.298	482.214	5.498	5.7766	0.09240
2176	479.305	482.249	5.446	5.7757	0.09304
2177	479.308	482.505	5.403	5.7735	0.09209
2178	479.315	482.665	5.373	5.7721	0.09283
2179	479.317	482.928	5.344	5.7700	0.09234
2180	479.328	483.147	5.318	5.7683	0.09238
2181	479.339	481.593	10.427	5.8402	0.09411
2182	479.334	481.676	10.402	5.8394	0.09478
2183	479.336	481.964	10.376	5.8373	0.09386
2184	479.336	482.035	10.350	5.8366	0.09481
2185	479.340	482.211	10.319	5.8351	0.09492
2186	479.334	482.261	10.255	5.8341	0.09476
2187	479.339	482.520	10.183	5.8317	0.09454
2188	479.351	482.625	10.124	5.8303	0.09477

Point ID	T_0	T_e	P_e	ρ_e	λ_e
	(K)	(K)	(MPa)	(mol·L^{-1})	(W·m^{-1}K^{-1})
2189	479.353	482.925	10.073	5.8279	0.09402
2190	479.353	483.031	10.023	5.8267	0.09497
2191	479.403	481.552	20.315	5.9461	0.09820
2192	479.409	481.624	20.242	5.9450	0.10000
2193	479.399	481.901	20.168	5.9427	0.09867
2194	479.407	482.010	20.095	5.9414	0.09926
2195	479.403	482.282	20.023	5.9391	0.09878
2196	479.408	482.377	19.949	5.9379	0.09882
2197	479.413	482.639	19.875	5.9357	0.09838
2198	479.413	482.653	19.774	5.9346	0.09905
2199	479.407	482.904	19.649	5.9319	0.09818
2200	479.416	483.002	19.538	5.9303	0.09894
2201	479.458	481.566	30.462	6.0404	0.10241
2202	479.454	481.624	30.311	6.0388	0.10355
2203	479.452	481.874	30.160	6.0362	0.10299
2204	479.452	481.988	30.012	6.0343	0.10449
2205	479.453	482.261	29.860	6.0316	0.10228
2206	479.453	482.360	29.714	6.0298	0.10333
2207	479.452	482.612	29.561	6.0271	0.10268
2208	479.453	482.568	29.377	6.0257	0.10369
2209	479.452	482.859	29.179	6.0224	0.10217
2210	479.456	482.955	28.998	6.0203	0.10205
2211	479.455	481.770	5.631	5.7812	0.09238
2212	479.450	481.848	5.634	5.7807	0.09312
2213	479.455	482.152	5.636	5.7788	0.09194
2214	479.461	482.276	5.631	5.7779	0.09279
2215	479.462	482.575	5.624	5.7759	0.09216
2216	479.466	482.713	5.618	5.7749	0.09297
2217	479.465	483.003	5.611	5.7729	0.09199
2218	479.467	483.121	5.602	5.7721	0.09322
2219	479.476	483.476	5.592	5.7697	0.09198
2220	479.480	483.619	5.582	5.7686	0.09290
2221	503.337	505.292	0.600	5.5473	0.08754
2223	503.349	505.683	0.568	5.5439	0.08694
2224	503.348	505.836	0.585	5.5430	0.08769
2225	503.350	506.203	0.606	5.5407	0.08714
2227	503.335	506.653	0.638	5.5380	0.08710
2228	503.323	506.788	0.648	5.5371	0.08755
2229	503.309	507.080	0.654	5.5351	0.08668
2230	503.302	507.128	0.657	5.5348	0.08750
2231	503.239	505.272	5.440	5.6239	0.08982
2232	503.246	505.381	5.428	5.6230	0.09063
2233	503.250	505.663	5.417	5.6209	0.08971
2234	503.264	505.761	5.406	5.6201	0.09005
2235	503.276	506.100	5.398	5.6177	0.08946
2237	503.291	506.146	5.320	5.6162	0.08965
2239	503.319	506.496	5.210	5.6122	0.08977
2240	503.334	506.649	5.175	5.6106	0.09002
2241	503.314	505.422	10.815	5.6982	0.09279
2242	503.297	505.568	10.787	5.6969	0.09268

Point ID	T_0	T_e	P_e	ρ_e	λ_e
	(K)	(K)	(MPa)	(mol·L^{-1})	(W·m^{-1}K^{-1})
2243	503.285	505.786	10.757	5.6951	0.09161
2244	503.274	505.895	10.725	5.6940	0.09251
2245	503.266	506.034	10.695	5.6928	0.09206
2246	503.258	506.099	10.663	5.6919	0.09264
2247	503.252	506.415	10.633	5.6896	0.09207
2248	503.251	506.548	10.604	5.6883	0.09300
2249	503.248	506.843	10.575	5.6861	0.09234
2250	503.255	506.991	10.546	5.6848	0.09264
2251	503.305	505.055	15.249	5.7565	0.09408
2252	503.311	505.242	15.219	5.7551	0.09493
2253	503.312	505.544	15.191	5.7530	0.09416
2254	503.306	505.689	15.159	5.7517	0.09472
2255	503.295	505.950	15.122	5.7497	0.09423
2256	503.284	506.061	15.083	5.7486	0.09488
2257	503.276	506.342	15.040	5.7464	0.09428
2258	503.266	506.470	14.994	5.7451	0.09466
2259	503.250	506.688	14.948	5.7432	0.09415
2260	503.244	506.881	14.899	5.7414	0.09487
2261	503.030	504.977	21.321	5.8270	0.09670
2262	503.021	505.041	21.330	5.8268	0.09749
2263	503.023	505.315	21.338	5.8253	0.09693
2264	503.023	505.334	21.345	5.8253	0.09878
2265	503.029	505.429	21.321	5.8245	0.09730
2266	503.026	505.510	21.262	5.8234	0.09744
2267	503.029	505.765	21.220	5.8215	0.09681
2269	503.036	506.071	21.159	5.8191	0.09678
2270	503.036	506.201	21.135	5.8182	0.09722
2272	502.988	504.718	30.822	5.9257	0.10159
2273	502.993	504.954	30.785	5.9242	0.10101
2274	502.993	505.058	30.756	5.9234	0.10089
2275	503.000	505.329	30.746	5.9219	0.10062
2276	502.997	505.568	30.787	5.9211	0.10073
2277	502.990	505.947	30.827	5.9195	0.10076
2278	502.985	506.088	30.852	5.9190	0.10129
2279	502.978	506.368	30.865	5.9177	0.10062
2280	502.975	506.483	30.873	5.9172	0.10087